iScience

CellPress
OPEN ACCESS

Article

Miniaturized Fab' imaging probe derived from a clinical antibody: Characterization and imaging in CRISPRi-attenuated mammary tumor models

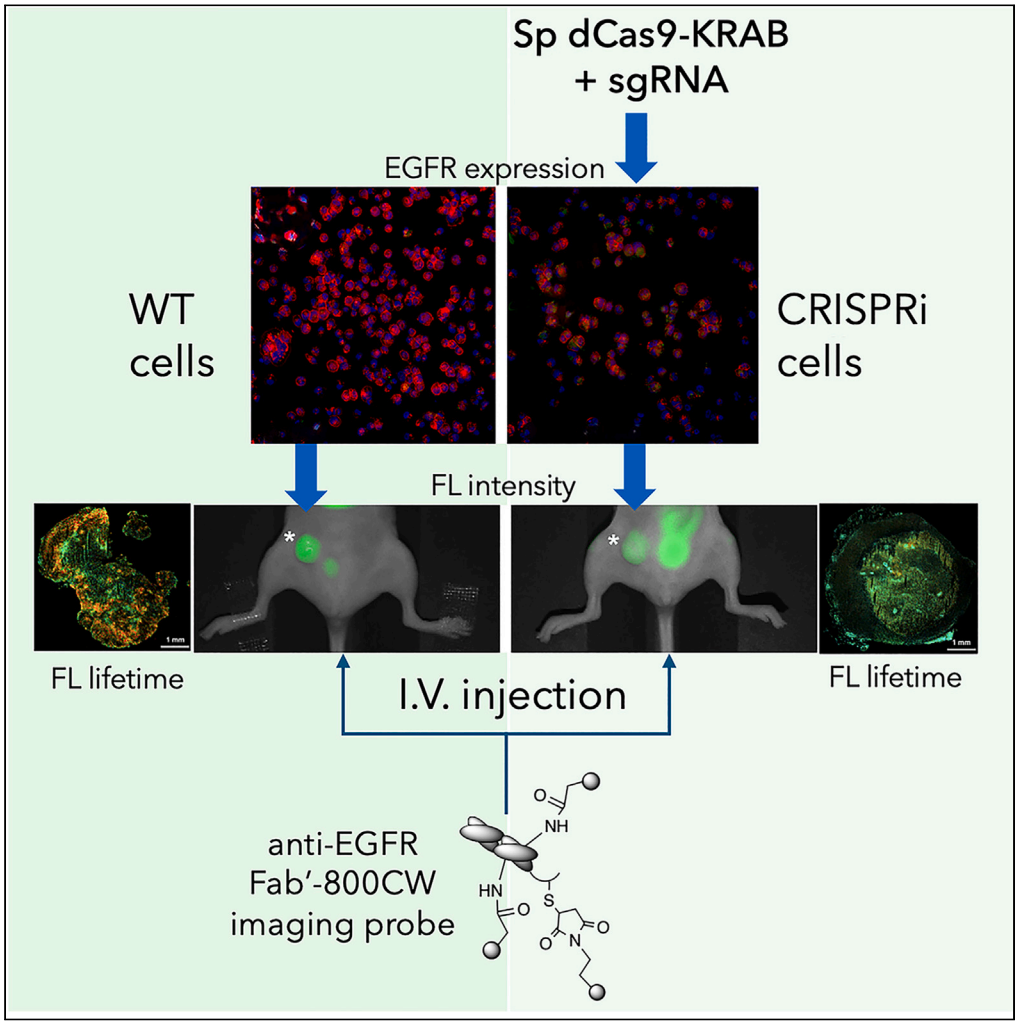

Suresh Gupta, Rahul Pal, Eric J. Schmidt, Murali Krishnamoorthy, Anita Leporati, Anand T.N. Kumar, Alexei Bogdanov, Jr.

alexei.bogdanov@umassmed.edu

Highlights

Both fluorescence intensity and lifetime increase after fragmentation of the Fab' NIR probe

Fluorescence lifetime contrast increases upon internalization of Fab' NIR probe

CRISPRi yielded two times lower EGFR expression in triple-negative breast cancer cells

Fab' probe showed the feasibility of CRISPRi effect imaging *in vivo* at an early time point

Gupta et al., iScience *27*, 110102
August 16, 2024
https://doi.org/10.1016/j.isci.2024.110102

iScience

CellPress
OPEN ACCESS

Article

Miniaturized Fab' imaging probe derived from a clinical antibody: Characterization and imaging in CRISPRi-attenuated mammary tumor models

Suresh Gupta,[1] Rahul Pal,[2,3] Eric J. Schmidt,[1] Murali Krishnamoorthy,[2,3] Anita Leporati,[1] Anand T.N. Kumar,[2,3] and Alexei Bogdanov, Jr.[1,4,5,*]

SUMMARY

Clinical imaging-assisted oncosurgical navigation requires cancer-specific miniaturized optical imaging probes. We report a near-infrared (NIR) Fab'-based epidermal growth factor receptor (EGFR)-specific probe carrying 3 NIR fluorophores (Fab'-800CW), which retained high-affinity binding to EGFR ectodomain (equilibrium K_D^E = 1 nM). Fab'-800CW showed a robust 4-times gain of fluorescence intensity (FI) and a 20% lifetime (FLT) increase under the conditions mimicking intracellular degradation. The probe was tested by using triple-negative breast cancer (TNBC) cell lines obtained by applying CRISPR interference (CRISPRi) effect of *EGFR*-targeting sgRNA and dCas9-KRAB chimera coexpression in MDA-MB-231 cells (WT cells). FI imaging in cell culture proved a 50% EGFR expression attenuation by CRISPRi. FI imaging in animals harboring attenuated or WT TNBC tumors with *ex vivo* corroboration identified differences between WT and CRISPRi tumors FI at 30 min post injection. Our results suggest the feasibility of EGFR expression imaging using a Fab'-based probe relevant for imaging-guided cancer surgery.

INTRODUCTION

The development of both improved optical imaging probes and novel realistic models of cancer currently are among the most important goals of translational cancer research and it is driven, in part, by the needs of more accurate optical imaging–guided surgical resection of tumors.[1] Fluorescence-based approaches are especially attractive due to molecular specificity of optical imaging combined with the lack of exposure to ionizing radiation, which may be integrated with surgical suite modalities for non-contact monitoring of tissue fluorescence.[2–5]

We previously demonstrated that imaging signal amplification in both planar and 3D tomographic imaging setups may be successfully used for imaging cell-surface targets, which are critically important in precision oncology.[6–8] Some signal amplification strategies rely on enzyme-mediated signal generation occurring via oligomerization and retention of paramagnetic and fluorescent imaging quasi-substrates in the target tissues.[6,9–11] Alternatively, optical imaging signal is generated due to the intracellular enzymatic conversion of poorly fluorescent quenched macromolecular precursors (imaging substrates[12,13] as well as reactive activity probes[14,15]) into fluorescent products that emit low energy (near-infrared, NIR) photons. This has important practical implications because these photons are less prone to absorption and scattering *in vivo*.[16,17] Importantly, NIR fluorophores, which are currently used in clinical trials,[18–20] can be linked to cancer specific antibodies enabling specific cancer cell imaging with optical signal amplification.[21,22]

Exogenous macromolecular optical imaging substrates (targeted or non-targeted) are internalized by live mammalian cells via endocytosis or pinocytosis and undergo degradation by the enzymes of the endolysosomal compartment.[23] The resultant products not only display fluorescence intensity (FI) exceeding that of the initial substrate but may also result in significantly longer fluorescence lifetimes (FLT) of linked fluorophores.[7,8,24] The advantages of FLT time domain mode of imaging both *in vitro* and *in vivo*[25–27] include proportionality to the quantum yield and FLT independence of the fluorophore concentration at constant temperature.[28] Furthermore, the transition from short FLT of intact labeled macromolecule to fragmented state is associated with rapid FLT increase with the rate greatly exceeding the FI increase rate and resultant excellent FLT contrast.[8] The last aspect is important for clinical translation because in clinically relevant situations imaging procedures should be performed without the need of long waiting periods between injection and image acquisition.[29] For successful FLT imaging of cancer-specific antigens an imaging probe should have proven specificity and a capability of generating appropriate imaging contrast shortly after injection. Here we sought to pursue the following goals: (1) to develop a miniaturized NIR imaging probe derived from a therapeutic

[1]Department of Radiology, UMASS Chan Medical School, Worcester, MA, USA
[2]Mike Toth Head and Neck Cancer Research Center, Massachusetts Eye and Ear, Boston, MA, USA
[3]A. Martinos Center for Biomedical Imaging, Department of Radiology, Massachusetts General Hospital, Charlestown, MA, USA
[4]Cancer Center and Chemical Biology Interface Program, UMASS Chan Medical School, Worcester, MA, USA
[5]Lead contact
*Correspondence: alexei.bogdanov@umassmed.edu
https://doi.org/10.1016/j.isci.2024.110102

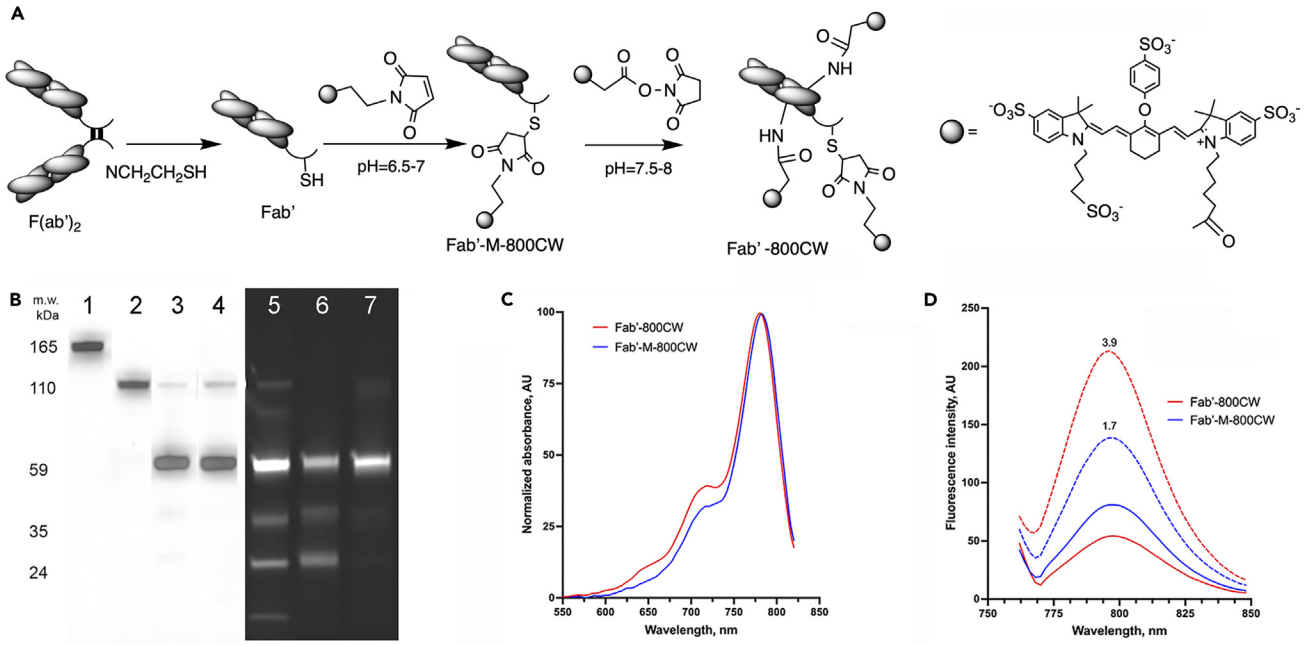

Figure 1. Synthesis and characterization of Fab'-800CW probe

(A) Synthesis of IRDye 800CW labeled Fab' fragment using orthogonal modification of thiols and amino groups. F(ab')$_2$ reduction with 2-MEA was followed by (1) blocking of cysteine thiols with IRDye 800CW maleimide and (2) modification of free amino groups by using IRDye 800CW NHS.

(B) SDS PAGE EF (4–15% gradient) of cetuximab IgG (lane 1), corresponding F(ab')$_2$ fragment (lane 2), IRDye 800CW – maleimide modified Fab' fragment (lanes 3,5), Fab' fragment after modification with both IRDye 800CW-maleimide and IRDye 800CW- NHS (lanes 4,6,7). SEC-HPLC purified Fab'-800CW probe is shown in the lane 7.

(C) Normalized absorbance spectra of Fab'-800CW.

(D) Fluorescence spectra (λ_{ex} = 700 nm). Traces corresponding to Fab'-*M*-800CW (Fab' modified with IRDye 800CW maleimide) is shown in blue; the spectra traces of Fab'-800CW (modified using both IRDye 800 CW maleimide and NHS ester) are shown in red; fluorescence spectra obtained after complete pepsinolysis (pH < 2, 3 h) are shown with dashed lines.

antibody by using orthogonal chemical reactions involving clinically translatable NIR fluorophores; (2) to test whether both FI and FLT of the probe change under conditions mimicking intracellular degradation; and (3) to obtain morphologically similar orthotopic mammary tumor models with diverse levels of relevant therapeutic target expression using CRISPR interference (CRISPRi) technique for *in vivo* testing of developed probe at early time points after systemic administration.

RESULTS

IRDye 800CW-conjugated Fab'

We used clinically available recombinant IgG (cetuximab) to generate miniaturized EGF receptor-specific probes. The synthesis involved the initial production of cetuximab F(ab')$_2$ fragment and followed the steps shown in Figure 1A. We performed a standard pepsinolysis of cetuximab IgG at pH 4 with optimization of reaction time followed by SEC-HPLC purification, which lead to high-purity F(ab')$_2$ (Figure 1B, lane 2). Further selective reduction of the hinge-region disulfide (cystine) bonds in the presence of 2-mercaptoethylamine (2-MEA) resulted in Fab' fragments carrying free thiols. The latter underwent facile covalent modification with IRDye 800 CW maleimide in the absence of oxygen. The treatment of reduced Fab' with IRDye 800CW maleimide resulted in a fluorescent product with only trace amounts of Fab' dimers present (Figure 1B). Though we anticipated the presence of two free SH groups per each Fab' molecule, linking of IRDye 800 CW maleimide resulted in one 800CW residue per Fab' fragment on the average (Fab'-*M*-800CW).

The obtained Fab'-*M*-800CW conjugate was subjected to further modification with IRDye 800CW N-hydroxysuccinimide (NHS) ester (Figure 1A), which gave a product with a total of 3 NIR fluorophores per Fab' as determined by specific absorbance of IRDye 800CW. After final HPLC purification the Fab' dimers as well as trace amounts of F(ab')$_2$ were separated giving the final NIR labeled imaging probe, i.e., Fab'-800CW (Figure 1D, lane 7). The results of further characterization of the probe by using Biacore-chip based assay, mass spectrometry (MS) of deglycosylated and reduced light chains (Lc), as well as Fd chain (the product of IgG heavy chain pepsinolysis) are summarized in Table 1. The affinity of Fab'-800CW to recombinant human EGFR ectodomain was compared to control N-ethylmaleimide (NEM) - modified Fab', as well as Cetuximab IgG. The comparison showed that the apparent K_D values reflecting EGFR antigen binding affinity of control Fab' and IgG single binding domain were similar (5.1 $\pm$ 1.5 vs. 4.9 $\pm$ 1.1 nM). The apparent K_D of Fab'-800CW was somewhat lower at 3.3 $\pm$ 0.5 nM (Table 1) and this value reflected slower association and dissociation under the conditions of chip assay. As expected, the equilibrium K_D of IgG

Table 1. Comparative properties of Cetuximab IgG, Fab' and Fab'-800CW

Sample	Lc mass, D	Fd mass, D	K_D^A, nM[b]	k_A $M^{-1}s^{-1}$ kinetic association constant	k_D s^{-1} kinetic dissociation constant	K_D^E, nM[c]
anti-EGFR IgG	–		4.9 ± 1.1	$9.5{\cdot}10^5$	$1.6.10^{-4}$	0.2
anti-EGFR Fab'[a]	23428	27374	5.1 ± 1.5[d]	$1.3{\cdot}10^6$[d]	$1.4.10^{-3}$[d]	1.1[d]
anti-EGFR Fab'-800CW	24409 (Lc+800CW)	29335 (Fd+2x800CW)	3.3 ± 0.5	$1.0{\cdot}10^6$	$1.1.10^{-3}$	1.0

[a]control Fab' was obtained by PNGase deglycosylation of $F(ab')_2$ followed by reduction with TCEP, and MS analysis.
[b]K_D^A, apparent dissociation constant was determined by using sensogram analysis (Biacore SPR, Cytiva) using 1:1 binding stoichiometry model, $n = 4$ concentrations of immobilized EGFR ectodomain. Data shown as mean ± SD.
[c]K_D^E – equilibrium dissociation constant was calculated as $K_D^e = k_D/k_A$.
[d]constants obtained by using NEM-modified dye-free Fab' fragment.

characterizing true affinity of the whole molecule was approximately 5-times higher than that of K_D of Fab'-800CW due to 10-times slower dissociation of IgG in comparison to monovalent Fab'.

The optical properties Fab'-800CW were further compared to maleimide-functionalized Fab'-*M*-800CW by recording absorbance and fluorescence spectra (Figures 1C and 1D). Normalized absorbance spectra of Fab'-800CW showed an 8–10% increase of optical density in the range of 675–725 nm. This spectral change is consistent with the blue-shifted H-dimers/aggregates formation,[30] which are more likely to form in solutions of Fab'-800CW, which carry several IRDye 800CW residues linked to the same Fab' molecule. Optical density measurements suggested that orthogonal Fab' modification reactions resulted in linking 3 molecules of 800CW to Fab'. The comparison of FI spectra of Fab'-800CW before and after complete pepsinolysis at pH < 2 (Figure 1D) showed that additional modification with IRDye 800CW NHS ester enables a robust increase of FI after complete pepsinolysis: the 2-step conjugation of three 800CW fluorophores per Fab' resulted in a NIR FI increase of 3.9–4.1-times vs. 1.9–2.1 increase of FI in the case of Fab'-*M*-800CW. Additional LC-MS characterization of deglycosylated and reduced Fab' chains supported the conclusion regarding 800CW conjugation stoichiometry since Lc of Fab'-800CW was found to carry one residue of the dye while Fd fragment of heavy IgG chain contained two residues (Table 1).

Stability of Fab'-800CW in plasma was assayed by incubating the probe in whole mouse plasma for 30 and 120 min at 37°C, i.e., over the time periods relevant for early time point imaging in animal models of cancer at concentrations corresponding to the initial concentration in blood (1 μM). NIR imaging analysis of the samples on SDS-PAGE gels after incubation showed that stability of Fab'-800CW was similar to IgG-800CW (Figure 2A) and did not change over a period of 2 h. The total fraction of 800CW-labeled fragments ranged between 6.4 and 7.5% of total fluorescence in both cases as determined by quantitative gel fluorescence analysis. Due to partial quenching and resultant blue-shifting Fab'-800CW probe showed blue-shifted fluorescence (yellow color on overlay of 700 and 800 nm channel images on Figure 2A). Probe degradation assays performed by using trypsin (T), pepsin (P) and GSH (G)-treated samples of purified 50 nM Fab'-800CW solutions (Figure 2B) showed that the probe was mostly resistant to trypsinolysis at 0.5 h with very minor fragmentation and only a small 10–18% increase of FI. Trypsinolysis resulted in a modest increase of average FLT by 60 ps (Figure 2C). In contrast to trypsinolysis, pepsin treatment resulted in fragmentation (Figure 2B, lane P) and lead to a robust increase of average FLT by 130 ps, i.e., from 0.43 ± 0.01 to 0.56 ± 0.01 ns in intact and pepsin-treated Fab'-800CW samples, respectively, Figure 2C (pseudocolor image) with a strong increase of FI (Figure 2C, lower image). Large excess of reduced glutathione (GSH) corresponding to the estimated intracellular concentration (7 mM,[31]) resulted in Fab'-800CW reduction to light and heavy chain fragments (Figure 2B, lane G) and produced strong increase in both average FLT by 120 ps and FI (a 170% increase), Figure 2C. Further analysis of protease-mediated fragmentation was performed by treating of Fab'-800CW probe with 6–10 U of human recombinant papain-like cysteine proteases, i.e., cathepsins K,L,B,S. Cathepsins K and B degraded about 50% of the probe in 30 min at 37°C due to the presence of corresponding endopeptidase cleavage sites (i.e., X(S/G)PGX and XRVVX preferred amino acid sequence specific cleavage sites, respectively[32]) of Cetuximab's light chain amino acid sequence as well as in N-terminal domains of the heavy chain (see Figure S1, Supplementary information).

Engineering and isolation of TNBC cells with attenuated EGFR expression

To generate cell lines expressing lower number of EGF receptors per cell than in parent TNBC MDA-MB-231 (WT) cells, we explored the use of stable expression of a combination of *S. pyogenes* (Sp) dCas9 endonuclease-KRAB repressor fusion protein, i.e., a catalytically inactive Sp Cas9 double mutant fused with a C-terminal Krüppel associated box (KRAB) domain,[33,34] and sgRNAs targeting *EGFR* gene. The analysis of human *EGFR* gene sequence revealed two promising targets for CRISPR interference in the 5′-flanking regions of the gene at −134 and −58 positions upstream of initiator codon and one target downstream of the GC-rich *EGFR* gene promoter (Figure 3A). These sgRNA-target DNA sequences (labeled as sgRNA2.1 and sgRNA3) are flanked with Sp dCas9-specific protospacer adjacent motif (PAM) on the non-target DNA strand. In addition, a single 20 nt sequence within the Exon II DNA sequence on (−) strand that could also be potentially targeted by dCas9/sgRNA complex was identified in a relative proximity of both *EGFR* promoter and intron-I containing a downstream enhancer sequence[35] (Figure 3, sgRNA1.1). Further, we performed transfection of wild-type MDA-MB-231 cells (WT) TNBC cells in the presence of a vector carrying a fragment encoding *dCas9-KRAB* positioned under the control of EF1a promoter and puromycin

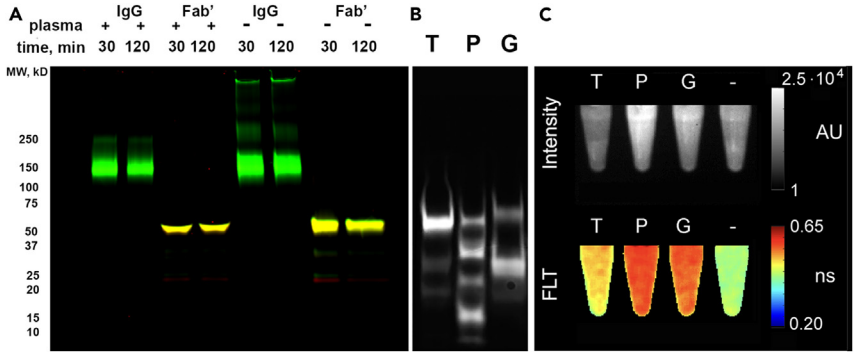

Figure 2. Stability of Fab'-800CW probe in plasma and susceptibility to degradation *in vitro*

(A) An overlay of fluorescent images obtained at excitation 700 nm (red) and 800 nm (green) of an 4–15% SDS PAGE gradient gel of IRDye 800CW labeled cetuximab (control, IgG) and cetuximab Fab'(experiment) incubated in the presence (+) or the absence (–) of mouse plasma concentration for 30 or 120 min at 37°C.

(B) NIR image (800 nm fluorescence detection) of an SDS PAGE gel with Fab'-800CW samples treated with: trypsin- (T), pepsin- (P), or reduced glutathione - (G).

(C) Fluorescence intensity (upper row) and fluorescence lifetime (pseudocolor image, lower row) of samples treated with trypsin (T), pepsin (P), reduced glutathione (G) at pH 7.5 for 30 min, as well as control sample (–). FI and FLT scales are shown next to the images. Protein staining of the gel shown in 2A panel is shown in Supplementary information (Figure S2).

resistance (Puro') cassette. Initial experiment using WT expressing a more potent dCas9 repressor-dCas9-KRAB-MeCP2[36] after transfecting with pLH sgRNA-coding vectors[37] did not yield stable clones. In contrast, expression of dCas9-KRAB and sgRNA1.1 (or sgRNA2.1, but not sgRNA3) in WT cells resulted in desired down-regulation in viable cells. As shown in Figure 3 (B and D, red fluorescence - AF647-labeled anti-EGFR mAb conjugate staining) CRISPRi-attenuated cells showed lower level of EGFR expression than in WT cells. This became apparent upon comparing relative FI of sgRNA2.1-expressing cells (shown in Figure 3 as a representative example of EGFR attenuation) and WT cells by using FACS analysis (Figures 3F and 3G). The levels of CRISPRi-unaffected PD-L1 expression (green fluorescence, Figures 3C–3E) in both populations of sgRNA2.1 vector-transfected cells that expressed EGFR at high and low levels (Figure 3G) were similar to the WT levels (Figure 3F).

Flow cytometry of cells isolated by using anti-EGFR Fab' sorting showed that EGFR-low expressing populations of both established cell lines co-expressing Sp dCas9-KRAB and sgRNA (named T2.1 and T2.2, respectively) comprised approximately 35% of total cells, with 65% of remaining cells displaying approximately 30% lower levels of EGFR-specific fluorescence than WT cells.

Quantitation of CRISPRi effect in EGFR-attenuated cell lines

The effect of CRISPRi downregulation of EGFR expression was characterized by performing Northern and Western blotting of total RNA and protein lysates, respectively (Figures 3H and 3I). The expression of EGFR mRNA in cell-isolated total RNA samples, which underwent testing by using a riboprobe with 100% complementarity to human EGFR mRNA, was compared by using total RNA isolated from WT, T1.1, T2.1 and mouse EMT6 tumor cell line. The complementarity of riboprobe to mouse EGFR mRNA sequence was 87%. Quantitation of total hybridized riboprobe signal showed that while human/mouse ratios in WT and T1.1 were similar, in T2.1 cells the ratio was 1.6 times lower ($p < 0.05$, Figure 3J). Western blotting with anti-human EGFR antibodies using cell protein lysates of WT, T1.1, and T2.1 cell lines showed that T2.1 cells expressed noticeably less EGFR corresponding to approximately 58% of GAPDH-normalized WT EGFR expression levels ($p < 0.05$), Figure 3I. Since EGFR expression in T2.1 cell was significantly lower both at the level of *EGFR* transcripts and EGFR protein than in T1.1 cells, we chose to use T2.1 CRISPRi-attenuated EGFR expressing cell line in the most of further experiments.

Binding and processing of EGFR imaging probes by WT and CRISPRi - attenuated cell lines

Probe uptake tests were performed in cell culture of WT and T2.1 cells using the same range of Fab'-conjugated IRDye 800CW concentrations (0.4–100 nM). In the cell monolayer experiment Fab'-800CW was incubated in complete cell culture medium for 30 min resulting in the concentration-dependent FI of the wells with washed and lysed cells (Figure 4A, inset) reflecting the presence of cell-bound and internalized fluorophores. WT cells had approximately 2.2-times higher FI than T2.1 cells in the studied range of concentrations (Figure 4A), and in both cases the addition of a 5-fold excess of anti-EGFR F(ab')$_2$ resulted in a roughly 10-fold decrease in FI (Figure 3A, open symbols). In the presence of the endocytosis inhibitor (NEM) at near-saturating concentrations of Fab'-800CW (100 nM 800CW), there was less of the T2.1 cell-surface associated Fab'-800CW probe (77.8 $\pm$ 2.5%) than in the case of WT cells (90.7 $\pm$ 4.1%, $p < 0.05$) after a 30 min incubation (Figure 4A, inset). The extension of incubation time beyond the short-term, i.e., for up to 1.5 h (Figure 4B), more closely reflects the time course of probe uptake by live cells. Note that cell uptake data shown in Figure 4B is expressed in pmoles of Fab'-800CW probe binding/internalization per million of cells. Binding and internalization kinetics showed that the uptake of the probes by the cells was rapid and did not show any significant increase ($p > 0.05$) over the initial period of 1.5 h.

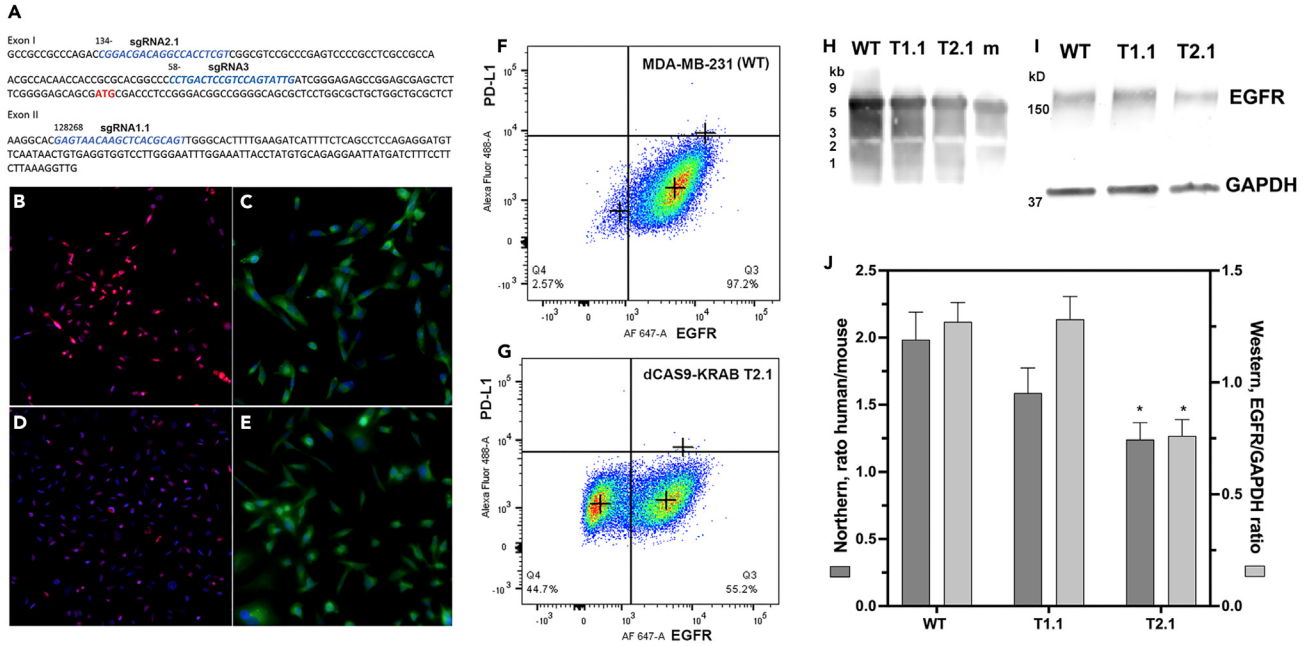

Figure 3. CRISPRi-mediated attenuation of EGFR expression in TNBC cells

(A) Fragments of human *EFGR* gene mRNA precursor (*EGFR* sequence (GenBank: X00588.1) corresponding to 5′ of Exon I and Exon II showing sgRNA target sequences (sgRNA1.1, 2.1 and 3.3, in blue). Translation initiation ATG codon is shown in red.

(B–E) Fluorescent microscopy of WT MDA-MB-231 cells (B, C) and CRISPRi EGFR-attenuated Sp dCas9-KRAB and sgRNA2.1 expressing cells (D, E). Dual channel fluorescent microscopy of EGFR (red- B, D, magnification −10x) and PD-L1 (green- C, E magnification 20x) cell surface expression. DAPI-stained nuclei are shown in blue.

(F and G) FACS analysis of EGFR and PD-L1 expression showing the appearance of CRISPRi EGFR-attenuated subpopulation of cells (panels G).

(H and I) Northern (H) and Western (I) blotting analysis of EGFR expression in WT cells and in T1.2 and T2.1 cells. Northern blotting was performed by probing total RNA isolated from cells with a 612 nt RNA Dig-labeled antisense RNA probe. m-negative control mouse RNA. EGFR detection on Western blots was performed by using anti-human EGFR and anti-GAPDH antibodies for blot normalization.

(J) Northern (dark gray bars) and Western (light gray bars) blotting signal quantitation. Asterisks indicate significant differences between the WT and T2.1 signal means ($p < 0.05$). Data shown as mean ± SD, $n = 3$.

The uptake of the probes by WT and CRISPRi *in vitro* by individual live cells (T2.1 and T1.1) was further analyzed by quantitative analysis of NIR fluorescence microscopy images acquired at two time points, i.e., 30 min corresponding to early probe binding and uptake phase (Figure 4C), and at 16 h (when probe internalization predominated), which was evidenced by high perinuclear and intra-nuclear FI (Figure 4C). The measurements of background- and noise-adjusted imaging signal averaged using 50–80 individual cells showed that the differences between the WT and CRISPRi cell groups were highly significant ($p < 0.01$) with approximately 2-times higher binding/uptake by WT cells observed at the early time point (30 min). The differences between SNR measured using WT and CRISPRi-attenuated cells were undetectable at 16 h.

While binding/uptake of Fab′-800CW probe by WT cells was clearly higher than in T2.1 cells (Figures 4A and 4B), the measured average NIR fluorescent signal in lysed cells is a result of multiple emitting populations of fluorophore with various average lifetimes. Fluorescence lifetime microscopy (FLIM) was performed using the cells fixed at approximately the same time points as for FI imaging (Figure 5). In general, during the initial internalization of the Fab′-800CW probe it redistributed from the surface to the endolysosomal compartment with the concomitant increase of FLT by 0.15–0.2 ns in both cell types. WT cells showed shorter FLT at 0.5 h in contrast to the T2.1 cells and had at least two populations of intracellular vesicles displaying shorter (0.3 ns) or longer (0.7 ns) lifetimes of the fluorophore. In both cell types the internalization of Fab′-800CW probe was evident at 16–18 h. At 18 h in WT cell culture there was mixed endolysosomal and nuclear fluorescence with predominantly longer FLT (0.8 ns). Unlike WT cells, their CRISPRi counterparts showed more rapid uptake and internalization of Fab′-800CW at the early (0.5 h) time point followed by probe redistribution to the nuclei, which displayed longer FLT (0.8–0.85 ns) at 18 h (Figure 4, arrows).

In vivo imaging of WT and EGFR CRISPRi tumor xenografts

Further, we determined whether Fab′-800CW imaging probe accumulation could be detected in experimental TNBC tumors *in vivo* at early time points after IV injection of 1.2 nmol Fab′-800CW/animal (approximately 3.6 nmol 800CW/animal), and whether imaging signal generated because of Fab′-800CW probe accumulation in WT and CRISPRi-attenuated tumors reflected the differences in EGFR expression. The FI NIR imaging of tumor xenografts developed after WT or T2.1 cell orthotopic implantation into the mammary fat pad of athymic (*nu/nu*) mice was

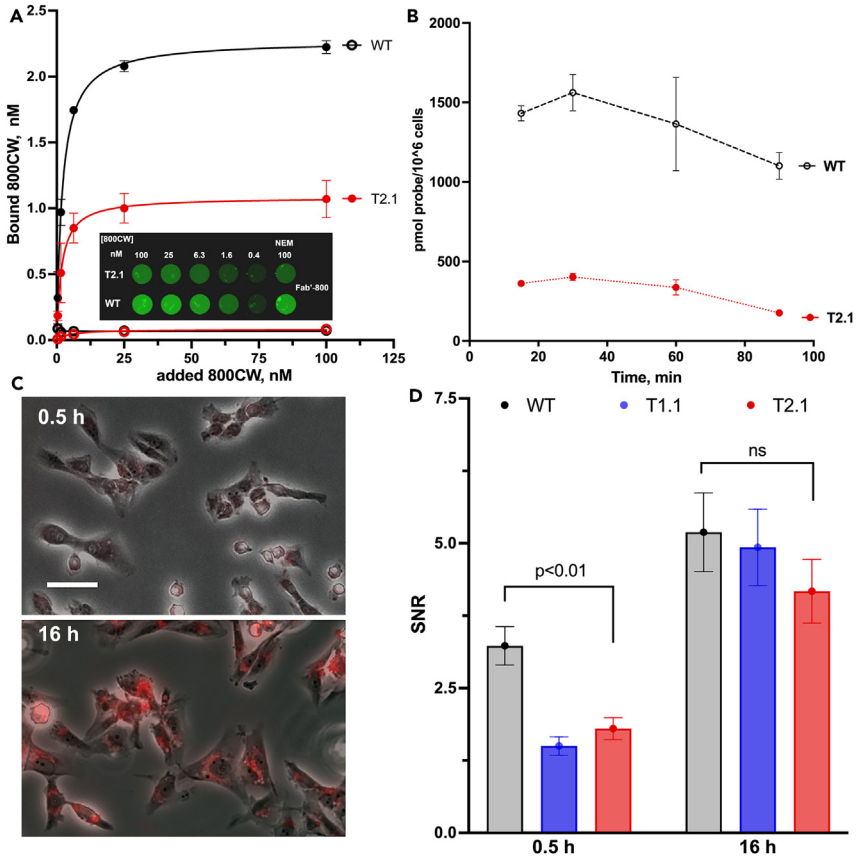

Figure 4. Binding and uptake of Fab'-800CW in T2.1 and WT cells

(A) Quantitation of the near-infrared fluorescence images of lysed cells incubated in the presence of serially diluted Fab'-800CW (0.4–100 nM of IRDye 800) in the absence (solid symbols) or in the presence (open symbols) of 5-fold excess of non-labeled $F(ab')_2$. Inset – a representative image of cell lysates in 96 well plate. The last column shows images of lysed cells pre-treated with 2 mM N-ethylmaleimide (NEM). Data shown as mean ± SD, $n = 3$.

(B) Time dependence of NIR imaging probe uptake (expressed in pmol of Fab'-800CW per million of cells). Data shown as mean ± SD, $n = 3$.

(C) Representative comparison of Fab'-800CW binding and uptake at early and late time points (0.5 and 16 h). Images show blended fluorescent (red) and phase (b/w) images of WT MDA-MB-231 cells after adding 200 nM Fab' −800CW to live cells. Bar = 20 μm.

(D) Quantification of fluorescence intensity bound/taken up by individual cells expressed as SNR-i.e., $(FI_{cell}\text{-}FI_{background})/SD_{background}$. Cell types: WT – gray, T1.1 – blue, T2.1 – red bars. Data in A, B, C is shown as mean ± SD, $n = 50$–80.

performed to obtain mean voxel intensity ratio calculated by analyzing standard constant-wave 2D FI images with tumor- and muscle placed ROIs. Analysis of these ROI ratios suggested that tumor FI, which exceeded background levels by a factor of 2 in both groups of animals, did not reveal significant differences between two groups including the endpoint imaging performed at 24 h (Figure 6A, $p > 0.05$). The NIR signal was detectable in the tumors beyond the initial 0.5 h time point and lasted at least for 24 h with tumor/background ratios improving over time (Figures 6C and 6D).

However, on CT-guided reconstructed 3D images of the same animals the total tumor fluorescence exhibited statistically significant differences ($p = 0.015$) between the T2.1 and WT groups at the early time point of 30 min post injection (Figure 6B). The mean FI of T2.1 tumors was lower by a factor of 2 in comparison to the WT tumors. Moreover, cross-section images of reconstructed volumes showed that FI of WT tumors could reach the level of at least an order of magnitude higher than FI of T2.1 tumors at the endpoint (Figures 6E and 6F).

Comparative qRT-PCR analysis of EGFR mRNA expression in cells and tumors

In vivo FI imaging data reflect the combination effect of (1) Fab'-800CW probe delivery to the tumor, (2) the binding to cells, and (3) the uptake by the cells of tumor microenvironment and resultant increase of FI due to fluorescence dequenching. Therefore, FI imaging results should depend in part on the levels of *EGFR* expression *in vivo*. We assessed these levels by performing comparisons of *EGFR* transcripts expression in each representative excised tumor of the WT and T2.1 (EGFR attenuated) animal groups. In both groups qRT-PCR analysis showed that for pairwise comparisons (12 pairs of animals), the majority of T2.1 tumors had lower normalized *EGFR* qRT-PCR signal than WT counterparts (Figure 7A; the ratio was lower than 0.95). Quantitative RT-PCR data acquired by using WT and T2.1 tumor cells confirmed the results of Western blotting of cell lysates (shown in Figure 3H), with normalized ratio of *EGFR* RT-PCR signals equal to 2.6 ± 0.2 (WT/T2.1, mean ± SD),

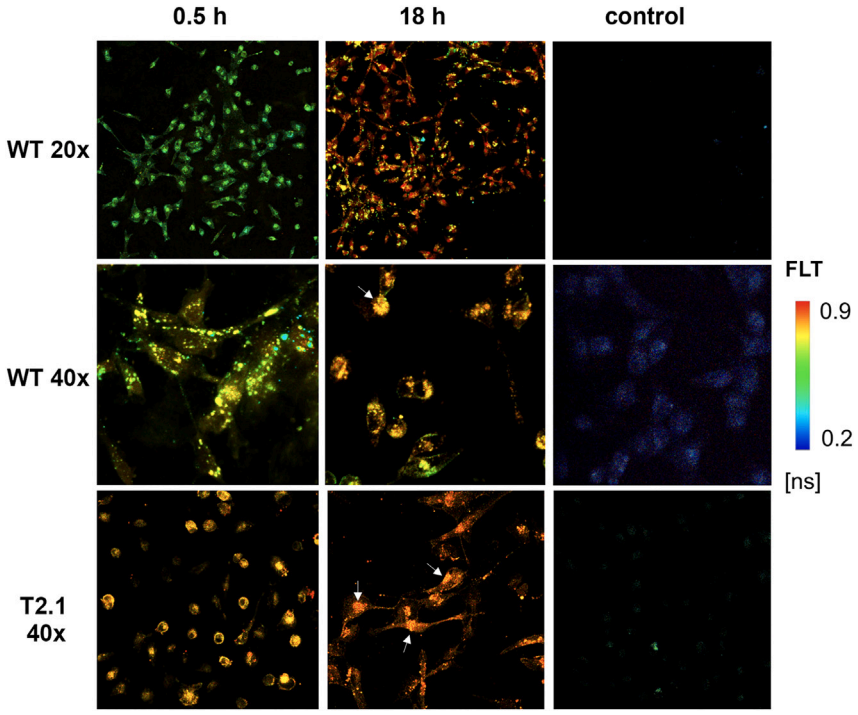

Figure 5. Fluorescence lifetime confocal microscopy of WT and T2.1 cells incubated with Fab'-800CW (50 nM IRDye 800CW) for 0.5 or 18 h in complete medium at 37°C

Nuclear uptake is shown with white arrows. FLT of control cells corresponded to autofluorescence levels. Cells were fixed and mounted in 50% glycerol before FLIM. Pseudocolor FLT scale is shown next to the images.

Figure 7B. In contrast, the same ratio determined for tumor-isolated total RNA was approximately 2 times lower (1.1 $\pm$ 0.1, $p < 0.01$), suggesting the presence of near-equal levels of *EGFR* transcripts in both types of tumors. Furthermore, the comparison of the ratios of *EGFR* RT-PCR signals determined in tumors vs. WT cancer cells showed that WT tumors expressed only 60% of *EGFR* transcripts present in WT cells. The difference of the means of qRT-PCR *EGFR* signals in WT and T2.1 tumors did not reach the level of statistical significance ($p = 0.07$), while T2.1 tumors contained 1.4 times more *EGFR* transcripts than T2.1 cells (Figure 7B).

Immunofluorescent and FLIM analysis of frozen tumor sections

Detailed characterization of WT and T2.1 tumor morphology (Figures 8A–8D) was performed by anti-EGFR and anti-CD31 antibody staining of thin sections to reveal the EGFR-positive tumor tissue and to estimate vascular density on the margin and within the whole tumor sections, respectively. Numerous CD31-positive blood vessels were detected at all tumor margins in both groups of animals. Image analysis of WT tumor sections (Figures 8A and 8B) revealed a well-developed blood supply with vascular density of 191 $\pm$ 87 vessels/mm^2. In contrast, only 84 $\pm$ 27 vessels/mm^2 were present across T2.1 tumor sections (Figures 8C and 8D), i.e., approximately 2-times lower than in the case of WT tumors. The average total area occupied by blood vessels per section showed very high variability, but the area with CD31-positive staining was higher on the average in the case of WT tumors - 9.6% (range: 5.5–13.5%) vs. 3.4% (range: 2.5–4.2%) in T2.1 tumors. This result indicated that T2.1 xenografts were on the average 3 times less vascularized.

Visualization of Fab'-800CW probe distribution within tumor sections of both animal groups was further performed by using a sensitive FLIM approach. Specific average fluorescence lifetime mapped over the total area of the WT tumors was longer than in T2.1 counterparts and approximately 0.2 ns longer than FLT of free (non-bound) Fab'-800CW, pointing to potential differences in binding, uptake, and processing of the probe by T2.1 vs. WT tumor cells as well as tumor-supporting stroma. The areas of tumor sections with longest fluorescence lifetimes - in the range of 0.9–1 ns in the case of WT and in the range of 0.5–0.6 ns in T2.1 tumor sections (Figures 8E and 8F) corresponded to vascularized regions. Additional higher resolution NIR microscopy showed perivascular accumulation of the probe in the same perivascular areas where CD31-positive endothelial cells were also identified (Figure S3).

DISCUSSION

Image-guided cancer surgery aided with a clinically approved antibody toolkit has the potential to drastically improve clinical outcomes due to improved accuracy of detecting residual cancer. Emerging evidence supports the development of intraoperative imaging probes that (1) detect their intended target shortly after systemic administration and (2) generate both FI and fluorescence lifetime contrast to take

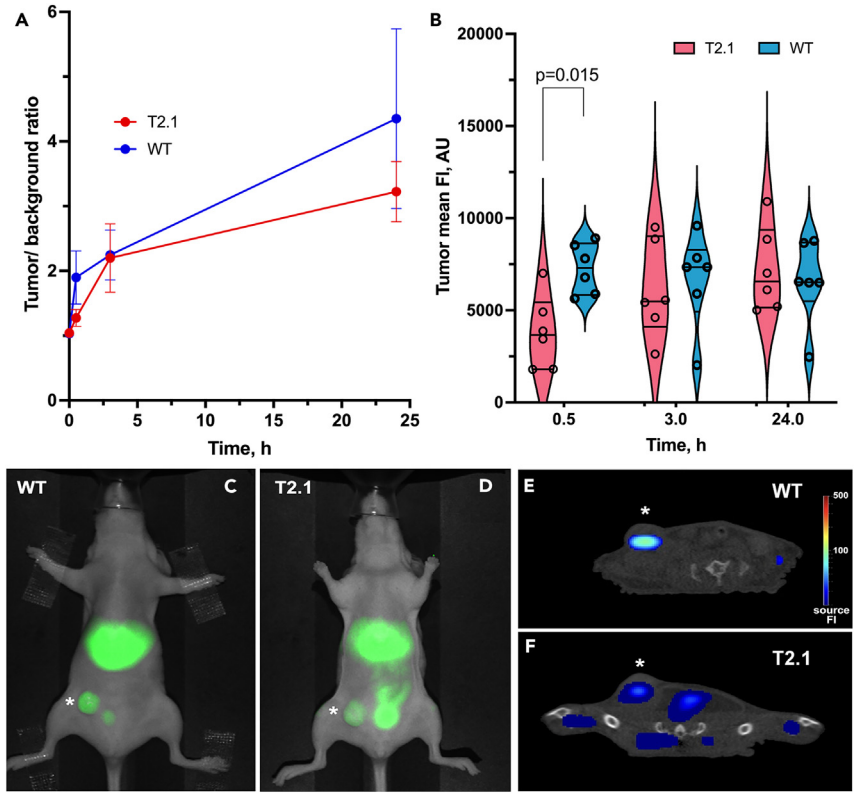

Figure 6. NIR fluorescent imaging of mice with WT and T2.1 xenografts after IV injection of 1.2 nmol Fab'-800CW/mouse (3.6 nmol IRDye 800CW/mouse)

(A) Results of planar (2D-constant wave) imaging with quantitation of tumor/background fluorescence ratio change over time using mean ROI voxel counts (background-skeletal muscle signal) data are shown as mean ± SD, $n = 6$.

(B) Violin plot showing the distribution of mean tumor fluorescence intensity at various time points, data are shown as mean ± SD, $n = 6$/group.

(C and D) Representative endpoint (24 h) planar fusion images of mice with WT-TNBC mammary tumor and CRISPRi T2.1- tumors, respectively.

(E and F) Cross-sectional (axial) fluorescence/CT fusion images (3D FLIT/CT) showing representative imaging slices obtained using mice implanted with WT control (E) and CRISPRi-attenuated T2.1 (F) tumors. Asterisks mark mammary tumor locations.

advantage of quantitative differences between imaging probe accumulation patterns in the tumors and in normal tissue. The advances in recombinant antibody-based cancer therapies continue to aid in developing of antibody-derived imaging probes for imaging-guided surgical procedures.[4] Unfortunately, clinically available NIR fluorescent cancer-specific IgGs such as FDA-approved NIR dye labeled monoclonal antibodies[18,38,39] commonly yield low tumor/background ratios.[20] Their use also requires long waiting times until the desired tumor fluorescence is achieved.[4] Protein engineering enabled the development of a wide variety of high affinity ligands such as antibody mimics and fragments varying in size and valency.[40,41] These smaller recombinant proteins or IgG fragments (e.g., Fab and scFav fusion proteins, reviewed in[41]) diffuse into the tumor more readily and may penetrate tumor tissue more rapidly as demonstrated previously in an ectopic cancer model.[42] According to classic simulations based on clinical blood plasma concentration profiles, in contrast to full-size IgG, much smaller Fab fragments should be capable to diffuse into deeper sites inside the tumors and achieve higher tumor concentrations than bivalent IgG or F(ab')$_2$ fragment at early times post injection.[43] The use of smaller imaging probes is underscored by clinical needs: early tumor-specific imaging in clinical setting would be highly desirable and serves as the major motivation for miniaturized probe development. The feasibility of shortening the imaging time window down to 10 h in a subcutaneous tumor model was previously demonstrated by using a recombinant anti-EGFR Fav-based enzymatically labeled fusion protein.[42] Probe optimization studies comparing side-by-side intact humanized IgG vs. IgG fragments labeled with NIR dyes suggest that experimental tumors could be imaged earlier, but at lower peak FI, by using antibody fragments (e.g., anti-HER3[44]) instead of a full-size IgG.[45]

Furthermore, applying time domain fluorescence lifetime imaging instead of constant wave excitation for FI imaging may yield major improvements in intraoperative cancer imaging. FLT is not affected by fluorophore concentration and excitation light intensity variations.[20,27,46] The increase of NIR fluorophore FLT in human tumors is diagnostic of the presence of residual cancer cells[47] and enables FLT-based differentiation of tumors and normal surrounding tissue (muscle) due to the difference between average tumor (0.70 ± 0.01 ns) and muscle (0.62 ± 0.01) FLT ($p < 0.05$). This statistically significant difference, measured by FLT imaging after 800CW-linked anti-EGFR probe injection, was sufficient for improving visualization of tumor margins,[46] which is critically important for improving surgery outcomes in cancer patients.[18]

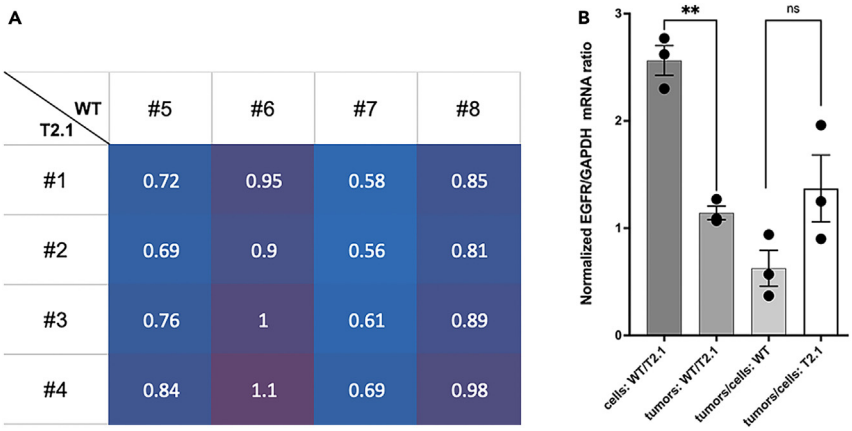

Figure 7. qRT-PCR comparative analysis of EGFR expression in WT and T2.1 cells and tumors

(A) The results are shown as pairwise (n = 16 pairs) heatmap comparisons of GAPDH-cDNA normalized EGFR of the WT and T2.1 CRISPRi-attenuated animal groups.

(B) The ratios comparing normalized EGFR qRT-PCR data obtained by using total RNA isolated from WT MDA-MB-231 cells, T2.1 cells and corresponding tumor xenografts. These comparisons show relative levels of *EGFR* expression *in vitro* as well as *in vivo*. Data presented as mean ± SD, n = 3. The differences between WT/T2.1 cell vs. WT/T2.1 tumor *EGFR* expression ratios were highly statistically significant ($p < 0.01$). The comparisons of tumor/cell expression ratios did not show statistically significant differences ($p = 0.1$).

Unlike Fab fragments of IgG, the use of Fab' in imaging has not yet been widely pursued. Meanwhile Fab' fragments can be readily synthesized by using multiple IgG subclasses.[48,49] Moreover, Fab' fragments carry both cysteine thiols and N-ε amino groups of lysines, which can be used for orthogonal chemical modification.[50] In this work we obtained Fab'-based NIR imaging probe labeled with multiple IRDye 800CW residues. These monovalent EGFR-specific Fab' NIR probes had about 3 times lower mass than the full-size IgG while their affinity (expressed as effective K_D) to EGFR ectodomain was preserved and comparable to K_D values of EGFR-specific single chain scFv,[51] single domain camelid antibody[52] and nanobody[53] that range between 4 and 40 nM. Two important *in vitro* observations supported further experiments involving Fab'- 800CW: (1) enzymatic degradation of Fab'-800CW imaging probe resulted in a 4-fold increase of FI and a 20% increase of average FLT of Fab'-conjugated IRDye 800CW fluorophores; (2) GSH mimicking an intracellular reducing environment produced significant increases of both FLT and FI. To assess quantitative differences between fluorescent signals in cells with various EGFR expression levels, we achieved EGFR expression attenuation by using CRISPRi technique. Standard MDA-MB-231 TNBC (WT) cell line with known EGF receptor expression (approximately $1{\cdot}10^5$ receptors/cell[54]) afforded an excellent target for CRISPRi since *EGFR* gene transcription is upregulated but not amplified in these cells. Because Fab'-800CW probe is monovalent, the binding and uptake in CRISPRi-attenuated cells is a function of receptor number rather than a combination of receptor number and receptor cell surface density/clustering affecting IgG binding/uptake. As expected, CRISPRi-attenuation of EGFR resulted in profound differences in FI between T2.1 cells and WT *in vitro* that were observed at early time periods during the co-incubation (Figure 5). Both FLIM and FI imaging of cells revealed more rapid internalization of Fab'-800CW in T2.1 cells than WT cells, indicating potential compensatory response to CRISPRi-attenuation of EGFR expression levels.

Further noninvasive *in vivo* imaging of EGFR-mediated probe uptake in the WT and CRISPRi tumors demonstrated that the difference between total mean WT vs. T2.1 tumor fluorescence observed early on (30 min) after the IV injection of the Fab'-800CW probe was transient (Figure 6). Total relative levels of *EGFR* gene expression in WT and T2.1 tumors exhibited tendencies that were opposite to those observed in respective cell lines (Figure 7). This finding confirmed less pronounced impact of CRISPRi on EGFR expression *in vivo*, even though most tumors in T2.1 group expressed less EGFR than the WT tumor group. The most plausible cause of higher FI of WT group observed early on after the IV injection is the presence of approximately 2-times higher density of blood vessels in the WT tumor group (Figure 8), with large surface area enabling more efficient transport of the imaging probe into the tissue. Large blood vessel wall area supports more avid early permeation (or "percolation"[43]) of Fab'-800CW into the tissue from the blood pool resulting in quantifiable differences revealed by optical image reconstruction obtained at 30 min after injection (Figure 6B).

Thus, our study explored an interdisciplinary approach focused on a novel miniaturized fluorescent probe developed by using clinically available antibody for enabling imaging-guided cancer surgery. The probe changes its fluorescent properties after fragmentation in cancer cells overexpressing the target receptor (EGFR). By using CRISPR interference technique we engineered TNBC cell lines with targeted attenuation of EGFR and demonstrated that the levels of cell fluorescence correlated with EGFR attenuation. Importantly, CRISPRi resulted in differential effects on fluorescence lifetime of the internalized probe, which in further imaging experiments demonstrated the feasibility of EGFR detection at an early point *in vivo*. Early time point imaging using clinically available antibody fragments potentially represents a substantial improvement achieved by adopting streamlined techniques of fluorescent imaging probe synthesis.

In conclusion, the results of our work indicate that: 1) orthogonal conjugation of NIR dyes to Fab' fragments results in a partially quenched, high-affinity probe, which produces higher FI and longer FLT upon enzymatic degradation and GSH reduction; 2) CRISPRi of EGFR in TNBC

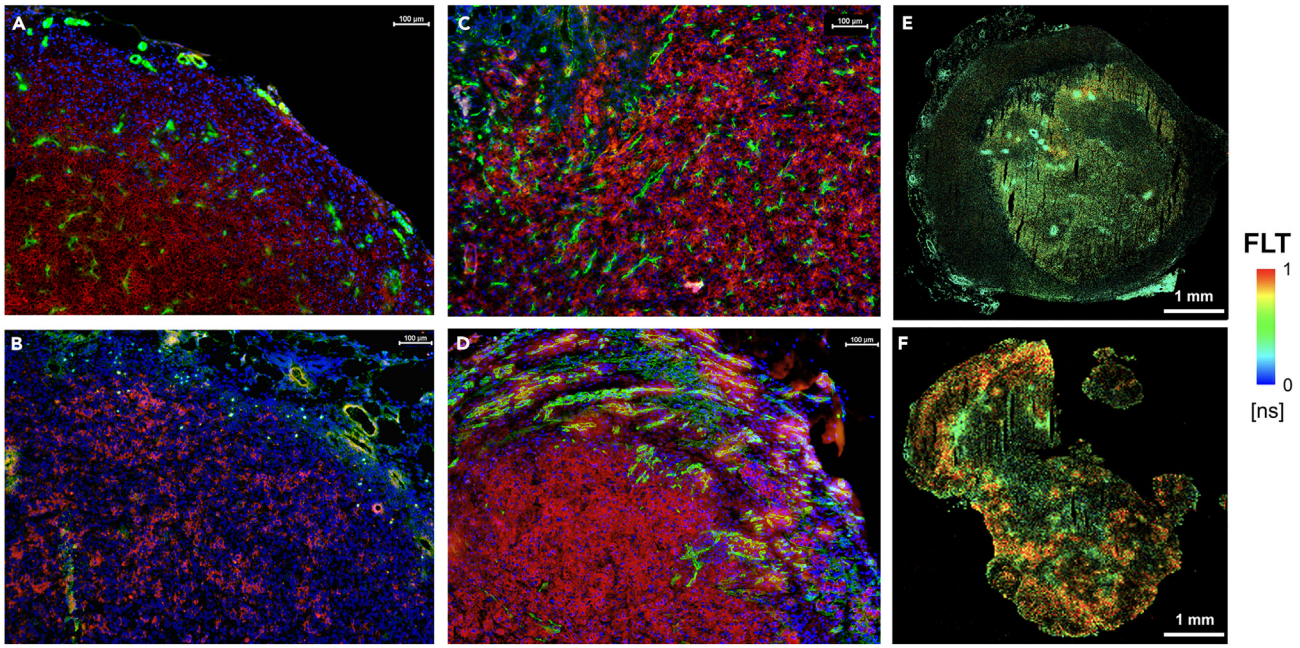

Figure 8. Immunofluorescent and FLIM analysis of thin frozen tumor sections

(A–D) Representative immunofluorescent microscopy of frozen sections of T2.1 (A and B) and WT (C and D) tumors. Green-anti-CD31, Red – anti-human EGFR, Blue – DAPI. Bar = 100 mcm.

(E and F) FLIM of frozen tumor sections, E– T2.1 tumor, F – wild-type tumor. Sections were post-fixed with 4% formaldehyde. Pseudocolor FLT scale is shown on the right. Bars (A–D) = 0.1 mm, bars (E, F) = 1 mm.

cell line resulted in attenuated EGFR expression; 3) *in vivo* NIR imaging by using anti-EGFR Fab'-800CW probe allowed FI imaging of WT and CRISPRi-attenuated experimental tumors at an early time point after systemic administration. Finally, fluorescence lifetime imaging of cells and tumor tissue suggested that internalized and fragmented anti-EGFR Fab'-800CW probe enhances FLT contrast. This finding is essential for developing future high-contrast imaging of receptor-mediated uptake based on FLT rather than FI during optically guided surgery of solid tumors. It is expected that multi-fluorophore probe-assisted, imaging-guided surgery would benefit from dual mode of fluorescence imaging, i.e., with both intensity- and lifetime contrast, the latter being actively developed into a clinical imaging modality.

Limitations of the study

There are several limitations to this study. While our work demonstrates facile synthesis of Fab'-based imaging probes which were effective in determining quantitative differences between the levels of EGFR expression in WT and CRISPRi attenuated cells, a wider panel of clinically available iso- and hetero-specific clinically available antibodies will have to be tested to select candidates with the best imaging characteristics for any given cancer-specific target. Certain limitation lies also in the need to perform a more detailed assessment of the degree to which the developed imaging probes retain specificity in the biological milieu. There were also limitations in the ability of CRISPRi to produce cell lines with desirable levels of stable attenuated expression of the target gene.

STAR★METHODS

Detailed methods are provided in the online version of this paper and include the following:

- KEY RESOURCES TABLE
- RESOURCE AVAILABILITY
  - Lead contact
  - Materials availability
  - Data and code availability
- EXPERIMENTAL MODEL AND STUDY PARTICIPANT DETAILS
  - Cell line
  - Animal model
- METHOD DETAILS
  - F(ab')$_2$ and IRDye 800CW-labeled Fab' preparation and characterization

- Proteolysis and stability of IRDye 800CW labeled Fab' antibody fragment
- Cell culture
- Vectors for CRISPRi and sgRNA
- Cell transfection
- FACS analysis
- Cell culture experiments
- RNA probe design, synthesis, and Northern blotting
- Fluorescence microscopy
- Fluorescence lifetime microscopy (FLIM)
- Widefield Fluorescence lifetime TD imaging
- Mouse model
- RNA extraction and qRT-PCR analysis
- Histology and immunohistochemistry

● QUANTIFICATION AND STATISTICAL ANALYSIS

SUPPLEMENTAL INFORMATION

Supplemental information can be found online at https://doi.org/10.1016/j.isci.2024.110102.

ACKNOWLEDGMENTS

NIH grants: This work was supported in part by NIH grants 2R01 EB000858 (to A.B.). R01 CA211084 (A.T.N.K.), R01 CA260857 (A.T.N.K.). We acknowledge the assistance of Shruti Choudhary (Sr. Research Scientist), UMASS Chan Small Molecule Screening, and Mass Spectrometry Facilities.

AUTHOR CONTRIBUTIONS

Conceptualization, A.B. and A.T.N.K.; Methodology, A.B., S.G., E.S., M.K., and A.L.; Investigation, A.B., S.G., and A.T.N.K.; Writing – Original Draft, A.B.; Writing – Review and Editing, A.B., S.G., R.P., E.S., A.T.N.K., M.K., and A.L.; Funding Acquisition, A.B. and A.T.N.K.; Resources, A.B. and A.T.N.K.; Supervision, A.B. and A.T.N.K.

DECLARATION OF INTERESTS

A.T.N.K. and R.P. are co-inventors of a pending US Patent application issued to The General Hospital Corporation. The patent might be the subject of a licensing agreement in the future. The authors declare no other competing interests.

Received: October 26, 2023
Revised: March 28, 2024
Accepted: May 22, 2024
Published: May 24, 2024

REFERENCES

1. Li, D., Zhang, J., Chi, C., Xiao, X., Wang, J., Lang, L., Ali, I., Niu, G., Zhang, L., Tian, J., et al. (2018). First-in-human study of PET and optical dual-modality image-guided surgery in glioblastoma using (68)Ga-IRDye800CW-BBN. Theranostics *8*, 2508–2520. https://doi.org/10.7150/thno.25599.
2. Crane, L.M.A., Themelis, G., Arts, H.J.G., Buddingh, K.T., Brouwers, A.H., Ntziachristos, V., van Dam, G.M., and van der Zee, A.G.J. (2011). Intraoperative near-infrared fluorescence imaging for sentinel lymph node detection in vulvar cancer: first clinical results. Gynecol. Oncol. *120*, 291–295. https://doi.org/10.1016/j.ygyno.2010.10.009.
3. Liu, Y., Zhao, Y.M., Akers, W., Tang, Z.Y., Fan, J., Sun, H.C., Ye, Q.H., Wang, L., and Achilefu, S. (2013). First in-human intraoperative imaging of HCC using the fluorescence goggle system and transarterial delivery of near-infrared fluorescent imaging agent: a pilot study. Transl. Res. *162*, 324–331. https://doi.org/10.1016/j.trsl.2013.05.002.
4. Pogue, B.W., Rosenthal, E.L., Achilefu, S., and van Dam, G.M. (2018). Perspective review of what is needed for molecular-specific fluorescence-guided surgery. J. Biomed. Opt. *23*, 1–9. https://doi.org/10.1117/1.JBO.23.10.100601.
5. Azari, F., Zhang, K., Kennedy, G.T., Chang, A., Nadeem, B., Delikatny, E.J., and Singhal, S. (2022). Precision Surgery Guided by Intraoperative Molecular Imaging. J. Nucl. Med. *63*, 1620–1627. https://doi.org/10.2967/jnumed.121.263409.
6. Shazeeb, M.S., Sotak, C.H., DeLeo, M., and Bogdanov, A. (2011). Targeted Signal-Amplifying Enzymes Enhance MRI of EGFR Expression in an Orthotopic Model of Human Glioma. Cancer Res. *71*, 2230–2239. https://doi.org/10.1158/0008-5472.Can-10-1139.
7. Bogdanov, A.A., Mazzanti, M., Castillo, G., and Bolotin, E. (2012). Protected Graft Copolymer (PGC) in Imaging and Therapy: A Platform for the Delivery of Covalently and Non-Covalently Bound Drugs. Theranostics *2*, 553–576. https://doi.org/10.7150/thno.4070.
8. Kumar, A.T.N., Rice, W.L., López, J.C., Gupta, S., Goergen, C.J., and Bogdanov, A.A., Jr. (2016). Substrate-based near-infrared imaging sensors enable fluorescence lifetime contrast via built-in dynamic fluorescence quenching elements. ACS Sens. *1*, 427–436. https://doi.org/10.1021/acssensors.5b00252.
9. Shazeeb, M.S., Gupta, S., and Bogdanov, A. (2013). MR Signal Amplification for Imaging of the Mutant EGF Receptor in Orthotopic Human Glioma Model. Mol. Imaging Biol. *15*, 675–684. https://doi.org/10.1007/s11307-013-0653-8.
10. Wadghiri, Y.Z., Hoang, D.M., Leporati, A., Gounis, M.J., Rodríguez-Rodríguez, A., Mazzanti, M.L., Weaver, J.P., Wakhloo, A.K., Caravan, P., and Bogdanov, A.A., Jr. (2018). High-resolution Imaging of Myeloperoxidase Activity Sensors in Human Cerebrovascular Disease. Sci. Rep. *8*, 7687. https://doi.org/10.1038/s41598-018-25804-y.

11. Bäuerle, T., Gupta, S., Zheng, S., Seyler, L., Leporati, A., Marosfoi, M., Maschauer, S., Prante, O., Caravan, P., and Bogdanov, A., Jr. (2021). Multimodal Bone Metastasis-associated Epidermal Growth Factor Receptor Imaging in an Orthotopic Rat Model. Radiol. Imaging Cancer *3*, e200069. https://doi.org/10.1148/rycan.2021200069.
12. Weissleder, R., Tung, C.H., Mahmood, U., and Bogdanov, A. (1999). In vivo imaging of tumors with protease-activated near-infrared fluorescent probes. Nat. Biotechnol. *17*, 375–378. https://doi.org/10.1038/7933.
13. Ntziachristos, V., Tung, C.H., Bremer, C., and Weissleder, R. (2002). Fluorescence molecular tomography resolves protease activity in vivo. Nat. Med. *8*, 757–760.
14. Blum, G., Mullins, S.R., Keren, K., Fonovic, M., Jedeszko, C., Rice, M.J., Sloane, B.F., and Bogyo, M. (2005). Dynamic imaging of protease activity with fluorescently quenched activity-based probes. Nat. Chem. Biol. *1*, 203–209. https://doi.org/10.1038/nchembio728.
15. Blum, G., von Degenfeld, G., Merchant, M.J., Blau, H.M., and Bogyo, M. (2007). Noninvasive optical imaging of cysteine protease activity using fluorescently quenched activity-based probes. Nat. Chem. Biol. *3*, 668–677. https://doi.org/10.1038/nchembio.2007.26.
16. Frangioni, J.V. (2003). In vivo near-infrared fluorescence imaging. Curr. Opin. Chem. Biol. *7*, 626–634.
17. Ntziachristos, V. (2010). Going deeper than microscopy: the optical imaging frontier in biology. Nat. Methods *7*, 603–614. https://doi.org/10.1038/nmeth.1483.
18. Korb, M.L., Hartman, Y.E., Kovar, J., Zinn, K.R., Bland, K.I., and Rosenthal, E.L. (2014). Use of monoclonal antibody-IRDye800CW bioconjugates in the resection of breast cancer. J. Surg. Res. *188*, 119–128. https://doi.org/10.1016/j.jss.2013.11.1089.
19. Gao, R.W., Teraphongphom, N., de Boer, E., van den Berg, N.S., Divi, V., Kaplan, M.J., Oberhelman, N.J., Hong, S.S., Capes, E., Colevas, A.D., et al. (2018). Safety of panitumumab-IRDye800CW and cetuximab-IRDye800CW for fluorescence-guided surgical navigation in head and neck cancers. Theranostics *8*, 2488–2495. https://doi.org/10.7150/thno.24487.
20. Pal, R., Hom, M.E., van den Berg, N.S., Lwin, T.M., Lee, Y.J., Prilutskiy, A., Faquin, W., Yang, E., Saladi, S.V., Varvares, M.A., et al. (2022). First Clinical Results of Fluorescence Lifetime-enhanced Tumor Imaging Using Receptor-targeted Fluorescent Probes. Clin. Cancer Res. *28*, 2373–2384. https://doi.org/10.1158/1078-0432.CCR-21-3429.
21. Hama, Y., Urano, Y., Koyama, Y., Choyke, P.L., and Kobayashi, H. (2007). Activatable fluorescent molecular imaging of peritoneal metastases following pretargeting with a biotinylated monoclonal antibody. Cancer Res. *67*, 3809–3817.
22. Hama, Y., Urano, Y., Koyama, Y., Kamiya, M., Bernardo, M., Paik, R.S., Shin, I.S., Paik, C.H., Choyke, P.L., and Kobayashi, H. (2007). A target cell-specific activatable fluorescence probe for in vivo molecular imaging of cancer based on a self-quenched avidin-rhodamine conjugate. Cancer Res. *67*, 2791–2799.
23. Bogdanov, A.A., and Mazzanti, M.L. (2013). Fluorescent Macromolecular Sensors of Enzymatic Activity for In Vivo Imaging. Prog. Mol. Biol. Transl. *113*, 349–387. https://doi.org/10.1016/B978-0-12-386932-6.00009-0.
24. Goergen, C.J., Chen, H.H., Bogdanov, A., Sosnovik, D.E., and Kumar, A.T.N. (2012). In vivo fluorescence lifetime detection of an activatable probe in infarcted myocardium. J. Biomed. Opt. *17*, 056001. https://doi.org/10.1117/1.JBO.17.5.056001.
25. Lakowicz, J.R. (1996). Emerging applications of fluorescence spectroscopy to cellular imaging: lifetime imaging, metal-ligand probes, multi-photon excitation and light quenching. Scanning Microsc. Suppl. *10*, 213–224.
26. Kumar, A.T.N., Skoch, J., Bacskai, B.J., Boas, D.A., and Dunn, A.K. (2005). Fluorescence-lifetime-based tomography for turbid media. Opt. Lett. *30*, 3347–3349.
27. Berezin, M.Y., and Achilefu, S. (2010). Fluorescence lifetime measurements and biological imaging. Chem. Rev. *110*, 2641–2684. https://doi.org/10.1021/cr900343z.
28. Time-Domain Lifetime Measurements (2006). In Principles of Fluorescence Spectroscopy, J.R. Lakowicz, ed. (Springer US), pp. 97–155. https://doi.org/10.1007/978-0-387-46312-4_4.
29. Sonn, G.A., Behesnilian, A.S., Jiang, Z.K., Zettlitz, K.A., Lepin, E.J., Bentolila, L.A., Knowles, S.M., Lawrence, D., Wu, A.M., and Reiter, R.E. (2016). Fluorescent Image-Guided Surgery with an Anti-Prostate Stem Cell Antigen (PSCA) Diabody Enables Targeted Resection of Mouse Prostate Cancer Xenografts in Real Time. Clin. Cancer Res. *22*, 1403–1412. https://doi.org/10.1158/1078-0432.CCR-15-0503.
30. Kobayashi, H., and Choyke, P.L. (2011). Target-cancer-cell-specific activatable fluorescence imaging probes: rational design and in vivo applications. Acc. Chem. Res. *44*, 83–90. https://doi.org/10.1021/ar1000633.
31. Montero, D., Tachibana, C., Rahr Winther, J., and Appenzeller-Herzog, C. (2013). Intracellular glutathione pools are heterogeneously concentrated. Redox Biol. *1*, 508–513. https://doi.org/10.1016/j.redox.2013.10.005.
32. Choe, Y., Leonetti, F., Greenbaum, D.C., Lecaille, F., Bogyo, M., Brömme, D., Ellman, J.A., and Craik, C.S. (2006). Substrate profiling of cysteine proteases using a combinatorial peptide library identifies functionally unique specificities. J. Biol. Chem. *281*, 12824–12832. https://doi.org/10.1074/jbc.M513331200.
33. Thakore, P.I., D'Ippolito, A.M., Song, L., Safi, A., Shivakumar, N.K., Kabadi, A.M., Reddy, T.E., Crawford, G.E., and Gersbach, C.A. (2015). Highly specific epigenome editing by CRISPR-Cas9 repressors for silencing of distal regulatory elements. Nat. Methods *12*, 1143–1149. https://doi.org/10.1038/nmeth.3630.
34. Lawhorn, I.E.B., Ferreira, J.P., and Wang, C.L. (2014). Evaluation of sgRNA target sites for CRISPR-mediated repression of TP53. PLoS One *9*, e113232. https://doi.org/10.1371/journal.pone.0113232.
35. Brandt, B., Meyer-Staeckling, S., Schmidt, H., Agelopoulos, K., and Buerger, H. (2006). Mechanisms of egfr gene transcription modulation: relationship to cancer risk and therapy response. Clin. Cancer Res. *12*, 7252–7260. https://doi.org/10.1158/1078-0432.CCR-06-0626.
36. Yeo, N.C., Chavez, A., Lance-Byrne, A., Chan, Y., Menn, D., Milanova, D., Kuo, C.C., Guo, X., Sharma, S., Tung, A., et al. (2018). An enhanced CRISPR repressor for targeted mammalian gene regulation. Nat. Methods *15*, 611–616. https://doi.org/10.1038/s41592-018-0048-5.
37. Ma, H., Naseri, A., Reyes-Gutierrez, P., Wolfe, S.A., Zhang, S., and Pederson, T. (2015). Multicolor CRISPR labeling of chromosomal loci in human cells. Proc. Natl. Acad. Sci. USA *112*, 3002–3007. https://doi.org/10.1073/pnas.1420024112.
38. Linssen, M.D., Ter Weele, E.J., Allersma, D.P., Lub-de Hooge, M.N., van Dam, G.M., Jorritsma-Smit, A., and Nagengast, W.B. (2019). Roadmap for the Development and Clinical Translation of Optical Tracers Cetuximab-800CW and Trastuzumab-800CW. J. Nucl. Med. *60*, 418–423. https://doi.org/10.2967/jnumed.118.216556.
39. Mulder, B.G.S., Koller, M., Duiker, E.W., Sarasqueta, A.F., Burggraaf, J., Meijer, V.E.d., Vahrmeijer, A.L., Hoogwater, F.J.H., Bonsing, B.A., van Dam, G.M., et al. (2023). Intraoperative Molecular Fluorescence Imaging of Pancreatic Cancer by Targeting Vascular Endothelial Growth Factor: A Multicenter Feasibility Dose-Escalation Study. J. Nucl. Med. *64*, 82–89. https://doi.org/10.2967/jnumed.121.263773.
40. Pluckthun, A., and Pack, P. (1997). New protein engineering approaches to multivalent and bispecific antibody fragments. Immunotechnology *3*, 83–105. https://doi.org/10.1016/s1380-2933(97)00067-5.
41. Iezzi, M.E., Policastro, L., Werbajh, S., Podhajcer, O., and Canziani, G.A. (2018). Single-Domain Antibodies and the Promise of Modular Targeting in Cancer Imaging and Treatment. Front. Immunol. *9*, 273. https://doi.org/10.3389/fimmu.2018.00273.
42. Kampmeier, F., Niesen, J., Koers, A., Ribbert, M., Brecht, A., Fischer, R., Kiessling, F., Barth, S., and Thepen, T. (2010). Rapid optical imaging of EGF receptor expression with a single-chain antibody SNAP-tag fusion protein. Eur. J. Nucl. Med. Mol. Imaging *37*, 1926–1934. https://doi.org/10.1007/s00259-010-1482-5.
43. Fujimori, K., Covell, D.G., Fletcher, J.E., and Weinstein, J.N. (1989). Modeling analysis of the global and microscopic distribution of immunoglobulin G, F(ab')2, and Fab in tumors. Cancer Res. *49*, 5656–5663.
44. El-Sayed, A., Bernhard, W., Barreto, K., Gonzalez, C., Hill, W., Pastushok, L., Fonge, H., and Geyer, C.R. (2018). Evaluation of antibody fragment properties for near-infrared fluorescence imaging of HER3-positive cancer xenografts. Theranostics *8*, 4856–4869. https://doi.org/10.7150/thno.24252.
45. Baart, V.M., van Manen, L., Bhairosingh, S.S., Vuijk, F.A., Iamele, L., de Jonge, H., Scotti, C., Resnati, M., Cordfunke, R.A., Kuppen, P.J.K., et al. (2023). Side-by-Side Comparison of uPAR-Targeting Optical Imaging Antibodies and Antibody Fragments for Fluorescence-Guided Surgery of Solid Tumors. Mol. Imaging Biol. *25*, 122–132. https://doi.org/10.1007/s11307-021-01657-2.
46. Pal, R., Kang, H., Choi, H.S., and Kumar, A.T.N. (2019). Fluorescence Lifetime-Based Tumor Contrast Enhancement Using an EGFR Antibody-Labeled Near-Infrared Fluorophore. Clin. Cancer Res. *25*, 6653–6661. https://doi.org/10.1158/1078-0432.CCR-19-1686.
47. Pal, R., Lwin, T.M., Krishnamoorthy, M., Collins, H.R., Chan, C.D., Prilutskiy, A., Nasrallah, M.P., Dijkhuis, T.H., Shukla, S., Kendall, A.L., et al. (2023). Fluorescence

lifetime of injected indocyanine green as a universal marker of solid tumours in patients. Nat. Biomed. Eng. *7*, 1649–1666. https://doi.org/10.1038/s41551-023-01105-2.

48. Ishikawa, E., and Yoshitake, S. (1980). A general and mild procedure for the purification of rabbit Fab' antibodies. J. Immunol. Methods *38*, 117–123. https://doi.org/10.1016/0022-1759(80)90336-1.
49. Garron, J.Y., Moinereau, M., Pasqualini, R., and Saccavini, J.C. (1991). Direct 99mTc labeling of monoclonal antibodies: radiolabeling and in vitro stability. Int. J. Rad. Appl. Instrum. B *18*, 695–703.
50. Ding, H., Carlton, M.M., Povoski, S.P., Milum, K., Kumar, K., Kothandaraman, S., Hinkle, G.H., Colcher, D., Brody, R., Davis, P.D., et al. (2013). Site specific discrete PEGylation of (124)I-labeled mCC49 Fab' fragments improves tumor MicroPET/CT imaging in mice. Bioconjug. Chem. *24*, 1945–1954. https://doi.org/10.1021/bc400375f.
51. Zhou, Y., Drummond, D.C., Zou, H., Hayes, M.E., Adams, G.P., Kirpotin, D.B., and Marks, J.D. (2007). Impact of single-chain Fv antibody fragment affinity on nanoparticle targeting of epidermal growth factor receptor-expressing tumor cells. J. Mol. Biol. *371*, 934–947. https://doi.org/10.1016/j.jmb.2007.05.011.
52. Rossotti, M.A., Henry, K.A., van Faassen, H., Tanha, J., Callaghan, D., Hussack, G., Arbabi-Ghahroudi, M., and MacKenzie, C.R. (2019). Camelid single-domain antibodies raised by DNA immunization are potent inhibitors of EGFR signaling. Biochem. J. *476*, 39–50. https://doi.org/10.1042/BCJ20180795.
53. Ding, L., Tian, C., Feng, S., Fida, G., Zhang, C., Ma, Y., Ai, G., Achilefu, S., and Gu, Y. (2015). Small sized EGFR1 and HER2 specific bifunctional antibody for targeted cancer therapy. Theranostics *5*, 378–398. https://doi.org/10.7150/thno.10084.
54. Yook, S., Cai, Z., Lu, Y., Winnik, M.A., Pignol, J.P., and Reilly, R.M. (2015). Radiation Nanomedicine for EGFR-Positive Breast Cancer: Panitumumab-Modified Gold Nanoparticles Complexed to the beta-Particle-Emitter, (177) Lu. Mol. Pharm. *12*, 3963–3972. https://doi.org/10.1021/acs.molpharmaceut.5b00425.
55. Wilkins, M.R., Gasteiger, E., Bairoch, A., Sanchez, J.C., Williams, K.L., Appel, R.D., and Hochstrasser, D.F. (1999). Protein Identification and Analysis Tools in the ExPASy Server. Methods Mol. Biol. *319*, 531–552. https://doi.org/10.1385/1-59259-584-7:531.
56. Chicaybam, L., Barcelos, C., Peixoto, B., Carneiro, M., Limia, C.G., Redondo, P., Lira, C., Paraguassú-Braga, F., Vasconcelos, Z.F.M.D., Barros, L., and Bonamino, M.H. (2016). An Efficient Electroporation Protocol for the Genetic Modification of Mammalian Cells. Front. Bioeng. Biotechnol. *4*, 99. https://doi.org/10.3389/fbioe.2016.00099.
57. Taghian, T., Metelev, V.G., Zhang, S., and Bogdanov, A.A., Jr. (2020). Imaging NF-κB activity in a murine model of early stage diabetes. FASEB J. *34*, 1198–1210. https://doi.org/10.1096/fj.201801147R.
58. Kocaturk, B., and Versteeg, H.H. (2015). Orthotopic injection of breast cancer cells into the mammary fat pad of mice to study tumor growth. J. Vis. Exp. *&squf*, 51967. https://doi.org/10.3791/51967.

STAR★METHODS

KEY RESOURCES TABLE

REAGENT or RESOURCE	SOURCE	IDENTIFIER
Antibodies		
Cetuximab (Erbitux)	Bio X Cell	SIM0002; RRID:AB_2894723
anti-EGF Receptor (D38B1) XP Rabbit mAb	Cell Signaling Technology	4267; RRID:AB_2246311
anti-GAPDH mAb 6C5	Abcam	ab92412; RRID:AB_2278693
anti-PD-L1-AF 488 (D8T4X) extracellular domain specific	Cell Signaling Technology	25048; RRID:AB_2798894
InVivoMAb anti-human PD-L1, B7-H1	Bio X Cell	BP0101; RRID:AB_2934050
anti-CD31/PECAM-1 MEC 13.3	Santa Cruz	sc-18916; RRID:AB_627028
anti-digoxigenin Fab	Roche	11214667001; RRID:AB_514494
anti-digoxigenin Fab, alkaline phosphatase conjugate	Roche	11093274910; RRID:AB_514497
goat anti-rabbit alkaline phosphatase conjugate	Sigma-Aldrich	A3687; RRID:AB_258103
mouse anti-rat IgG2a-AF488 (2A8F4)	Abcam	ab172332; RRID:AB_2893134
Chemicals, peptides, and recombinant proteins		
2-aminoethanthiol	Sigma-Aldrich	30070
IRDye® 800CW maleimide	Li-Cor	929–80021
IRDye® 800CW NHS ester	Li-Cor	929–70021
AlexaFluor™647 C2 Maleimide	Thermo-Fisher Scientific	A20347
Glutathione	Sigma-Aldrich	G4251
TRIzol	Thermo-Fisher Scientific	15596026
Tris(2-carboxyethyl) phosphine hydrochloride, TCEP	Thermo-Fisher Scientific	T2556
cOmplete™ mini EDTA-free Protease inhibitor cocktail	Roche-Millipore-Sigma	11836170001
ULTRAhyb™ Ultrasensitive Hybridization Buffer	Thermo-Fisher Scientific	AM8670
Pepsin A	Worthington Biochemical Corp	LS003319
Cathepsin K	AbCam	ab285940
Cathepsin L	AbCam	ab81780
Cathepsin S	AbCam	ab285884
Cathepsin B	AbCam	ab285903
EGFR ectodomain	Acro Biosystems	EGR-H5222
Deposited data		
In vivo fluorescence intensity ratio data	Mendeley data	https://doi.org/10.17632/dzn22c79nm.1
Software and algorithms		
ProtParam	Expasy.org	https://web.expasy.org/protparam/
MassLynx	Waters	N/A
ImageJ2(Fiji)	Open source	github.com/fiji/fiji
CRISPR design tool	Synthego	N/A
Other		
Superdex 200 Increase 10/300	Cytiva/GE Healthcare	28990944
CM5 Biacore Chip	Cytiva	29149604
Nucleofector 2b device	Lonza	AAB-1001
Ivis Spectrum CT	Revvity health Science Inc.	128201
Odyssey DLx Imager	Li-Corp	20541
FACSAria IIu	Beckton-Dickinson	P07800142

(*Continued on next page*)

Continued

REAGENT or RESOURCE	SOURCE	IDENTIFIER
BioRad 1000 series Thermal cycler	Bio-Rad	1851138
Vivaspin 4, 50,000 MWCO	Sartorius	VS04T31
Bio-Spin® 6 mini-columns	Bio-Rad	7326002
Amicon™ Ultra-4 Centrifugal Filter Units, 30,000 MWCO	MilliporeSigma™	UFC803008
Plasmid Miniprep kit	Qiagen	27104
Qiagen RNeasy Mini Kit	Qiagen	74104
High Pure PCR Product Purification Kit	Roche	1732668001
Maxima First Strand cDNA Kit with dsDNAse	Thermo-Fisher Scientific	K1671
HiFi 1st Strand cDNA synthesis kit	101 Bio.com	W2569

RESOURCE AVAILABILITY

Lead contact

All requests for resources and additional inquiries related to reagents should be directed to and will be handled by the lead contact: Alexei Bogdanov (alexei.bogdanov@umassmed.edu).

Materials availability

Synthetic steps and Fab' probe characterization are included in STAR methods. Additional probe characterization data and microscopy are provided in the supplemental information. Cell lines, antibodies and other biochemicals were acquired from commercial sources and are listed in the key resources table. New generated materials of this study are available upon request and MTA agreement.

Data and code availability

- Data: Original *in vivo* fluorescence intensity data have been deposited at Mendeley and are publicly available as of the date of publication. The DOI is listed in the key resources table. Microscopy data reported in this paper will be shared by the lead contact upon request.
- Code: No new code was generated in the process of this study.
- Additional information: Any additional information required to reanalyze the data reported in this paper is available from the lead contact upon request.

EXPERIMENTAL MODEL AND STUDY PARTICIPANT DETAILS

Cell line

Human triple-negative mammary adenocarcinoma MDA-MB 231 cell line (ATCC HTB-26) was obtained from the American Type Culture Collection (Manassas, VA, USA) and cultured according to the provided instructions.

Animal model

J:NU mice (n = 6/group, age: 5–6 weeks, sex: female, The Jackson Laboratory, Bar Harbor ME) were used for orthotopic mammary tumor propagation *in vivo* according to the protocol approved by The UMASS Chan Institutional Animal Care and Use Committee, IACUC protocol ID PROTO202200032.

METHOD DETAILS

F(ab')$_2$ and IRDye 800CW-labeled Fab' preparation and characterization

F(ab')$_2$ fragment using pepsin cleavage of the anti-EGFR chimeric monoclonal antibody (Cetuximab, ChiIgG1, Erbitux 2 mg/mL, *Merck Group*) was performed essentially as described in Shazeeb et al.[9] F(ab')$_2$ was purified using Superdex200 columns (10 × 300 mm, *Cytiva*) eluted with 0.1 M ammonium acetate, pH 7.0. F(ab')$_2$ was concentrated to 3 mg/mL (27 μM) on Vivaspin 4 50,000 MWCO ultrafiltration concentrators (*Sartorius*) and transferred into degassed and nitrogen-saturated 25 mM HEPES, 20 mM sodium tetraborate, 0.1 M NaCl (HBS-B) buffer containing 1 mM EDTA, pH 7.0. Stock solution of 2-aminoethanthiol (*Sigma-Aldrich*) was added to F(ab')$_2$ to achieve final concentration of 50 mM, flushed with argon and incubated at 37C for 2 h. Reduced F(ab')$_2$ (~54 μM Fab') was purified on Bio-Spin 6 mini-columns (*Bio-Rad*) equilibrated with degassed HBS-B, pH 7 as described by the manufacturer and IRDye 800CW maleimide (*Li-Cor*) was added to final concentration of 100 μM under argon and incubated for 12 h in the dark. To obtain Fab' with blocked thiols the Fab' fragment was modified with N-ethylmaleimide (NEM, 100 μM) using NEM instead of IRDye 800CW maleimide under the same conditions described above.

After adjusting pH to 8 using 1M sodium bicarbonate IRDye 800CW N-hydroxysuccinimide ester (5.2 mM in DMSO, *Li-Cor*) was added to final concentration of 150 μM and incubation continued for another 4 h. Purification of Fab'-800CW from free IRDye 800CW was achieved on Bio-Spin 30 mini-columns (*Bio-Rad*). Final purification was achieved by using Superdex200 columns as described above and the fractions containing pure Fab'-800CW probe were concentrated using 30,000 MWCO membrane concentrators (Amicon Ultra-4, *EMD-Millipore*). The purity was verified by 4–15% gradient SDS-PAGE. Routine concentration measurements were performed assuming extinction coefficients of Fab' (m.w. 55 kD) to be $\varepsilon^{0.1\%}_{280\ nm} = 1.54$, $\varepsilon_{280\ nm} = 72800\ M^{-1}\ cm^{-1}$ (ProtParam tool[55]) and IRDye 800CW $\varepsilon_{780\ nm} = 270{,}000\ M^{-1}\ cm^{-1}$.

Anti-EGFR Fab'-AF647 was prepared using $F(ab')_2$ reduction as described above by using Alexa Fluor 647 maleimide (*ThermoFisher*) modification of reduced and purified Fab' fragments. Labeled conjugates were stored at −20°C in HBS-B,50% glycerol, pH 7.

Biacore SPR (Cytiva) assays were performed by using recombinant EGFR ectodomain (*Acro Biosystems*) immobilized on the CM5 chip (*Cytiva*) by using water-soluble carbodiimide at 4 different concentrations: 50 μg/mL, 25 μg/mL, 12.5 μg/mL, and 6.25 μg/mL (approximately 500–62.5 nM). After immobilization, each antibody was titrated at 8 concentrations: 64, 32, 16, 8, 4, 2, 1 and 0.5 nM. The run included 300 s contact time with the analyte, 900 s dissociation time with a flow rate of 10 μL/min, 2 regeneration steps with 10 mM glycine, pH 2.5 for 10 s, flow rate 10 μL/min. The sensograms were analyzed using manufacturer-provided software using 1:1 binding model to calculate apparent K_D values. Kinetic constants (k_A, k_D) were determined using a chip channel with single concentration of immobilized EGFR (62.5 nM for conjugation).

Mass spectrometry analysis of samples was performed after deglycosylation and TCEP reduction. Two μg (0.1 μg/mL in water) of each sample were de-glycosylated by mixing with 4μL of Rapid PNGaseF buffer (5X) (*New England Biolabs, NEB*) and 1μL of Rapid PNGaseF (*NEB*) in a total volume of 20 μL, and incubating for 10 min at 50°C. One μL of each diluted sample (0.1 μg/μL), with and without PNGaseF were treated with 0.1 mM TCEP, and injected into the column (BioResolve RP mAB, (2.1 × 100 mm, 2.7 μm particle size) of LC-MS system (Waters Acquity UPLC coupled to Waters Synapt G2-Si QToF (Positive ESI), *Waters* and analyzed by using a gradient of acetonitrile in 0.1% formic acid in water. Each resultant LC peak was deconvoluted using the MaxEnt1 software (*Waters*). The range 20,000 to 35,000; 45000–55000 and 90000–110000 was used for output masses with the Uniform Gaussian damage model, employing a 1 Da width at half height, iterated to convergence.

Proteolysis and stability of IRDye 800CW labeled Fab' antibody fragment

Complete proteolysis of Fab' was accomplished by treating of IRDye 800CW labeled proteins with pepsin A solution (3.5 μg/mL final concentration, *Worthington Biochemical Corp*) in 0.1 sodium acetate, pH 2 and incubating for 3 h at 37°C. Fluorescent spectra of digested and intact conjugates were recorded in DPBS/methanol (1:1) to decrease weak interactions between IRDye 800CW residues. Treatment of 10 μL of 50 nM solutions of IRDye 800CW labeled Fab' antibody fragment with human recombinant cathepsins (B, K, L and S, 2–3 U of human recombinant catalytically active enzymes/sample, *BioVision/AbCam*) was performed in 20 μL 25 mM Mes, 50 mM KH_2PO_4, pH 5.5 for 2 h at 37°C. Trypsinolysis was performed by using 5 μg trypsin (typeIX-S, 14 U/μg, Sigma-Aldrich) as described above. Treatment with 7 mM reduced glutathione (GSH, *Sigma-Aldrich*) or 0.1 mM TCEP (*Thermo-Fisher*) was performed in DPBS, pH 7.0 and reaction was stopped by adding 5 mM N-ethylmaleimide. The samples were analyzed using SDS-PAGE (4–15% gradient) and quantified after imaging on Odyssey DLx Imager (*Li-Cor Corp*).

Cell culture

MDA-MB 231 (wild-type, WT) cells were purchased from the American Type Culture Collection (*ATCC* HTB-26). Cells were maintained in Lebovitz's L-15 media (*Gibco*) supplemented with 10% fetal bovine serum (*Hyclone*), penicillin (100 IU/mL), and streptomycin (50 μg/mL). Cells were subcultured 2 days before nucleofection and were ~80% confluent on the day of transfection. Stable clones of cells transfected with CRISPRi system were maintained in 10%FCS, Lebovitz's L-15, or 10%FCS DMEM in the presence of puromycin and hygromycin as described below.

Vectors for CRISPRi and sgRNA

dCas9-KRAB vector *Applied Biological Materials Inc.* (ABM: Cat #K203) and dCas9-KRAB-MeCP2, *Addgene* (#110821, [36]) were maintained in Stbl3 *E.Coli* (*Invitrogen* Cat #C7373-03) sgRNA sequences were designed by using human mRNA for precursor of EGFR sequence (GenBank: X00588.1) as FASTA target for Synthego's CRISPR design tool (https://www.synthego.com/products/bioinformatics/crispr-design-tool) for SpCas9 NGG protospacer adjacent motif (PAM). Forward and reverse oligonucleotides for 3 sgRNAs (2 for (+) DNA strand and 1 for (−) DNA strand within DNA sequence flanking Exon I and within Exon II of *EGFR* sequence (see Figure 3A).

Three pairs of fwd and rev oligonucleotides containing 5′ and 3′ overhangs:

sgRNA1.1 target DNA sequence:

5′ ACCGGAGTAACAAGCTCACGCAGT 3′ 98(+)
5′ AAACACTGCGTGAGCTTGTTACTC 3′

sgRNA2.1 target DNA sequence:

5′ ACCGCGGACGACAGGCCACCTCGT 3′ 134(-)
5′ AAACACGAGGTGGCCTGTCGTCCG 3′

sgRNA3 target DNA sequence:

5′ ACCGCAATACTGGACGGAGTCAGG 3′ 58 (–)
5′ AAACCCTGACTCCGTCCAGTATTG 3′

were synthesized, annealed, treated with BbsI, and cloned into pLH-spsgRNA2 vector (*Addgene* #64114 [37]). Reaction mixes were transformed into the Stbl3 competent cells. Qiagen Plasmid Miniprep kits were used for isolating plasmids from ampicillin-selected colonies and the inserts were verified by sequencing using pLKO.1-Rseq primer.

Cell transfection

Cells were harvested with TryPLE Express reagent (Gibco Cat # 12605010). $1 \cdot 10^6$ cells were sedimented, the supernatant was removed, and the cells were resuspended in 0.1 mL of ISM Chica buffer.[56] 2 μg of dCas9-KRAB vector in 5uL of TE buffer were added to the cells with mixing. Cells were electroporated using Nucleofector 2b (*Lonza*) in sterile 0.2-cm cuvettes (*Mirus Biotech*) using X-13 mode. After transfection, cells were resuspended in 1 mL of pre-warmed 20% FCS L-15 medium. In 48 h cells electroporated with dCas9-KRAB vector were selected using puromycin (0.5 μg/mL, determined by using dose-response curve) to obtain stably transfected clones. Cells were propagated for about 2 weeks before performing nucleoporation with pLH-spsgRNA2 containing T1.1,T 2.1 or T3.1 sgRNA inserts.

dCas9-KRAB-MeCP2 vectors or control dCas9-3xGFP plasmid (*Addgene*[37] were co-transfected in MDA-MB-231 cells together with pLH-spsgRNA2 vectors. All cells transfected with pLH-spsgRNA2 were grown in the presence of hygromycin (500 μg/mL) for selecting positive clones.

FACS analysis

Cells were harvested using TryPLE Express reagent, washed by centrifugation, and the cell pellet was resuspended in ice-cold 1%BSA in DPBS, pH 7.4 at $5 \cdot 10^6$ cells/mL. For fluorescent staining cells, 100 μL of cell suspension was transferred to 1.5 mL centrifuge tubes, primary pre-labeled antibodies (anti-EGFR- $F(ab')_2$-AF 647 and/or anti-PD-L1-AF 488 (#D8T4X, *Cell Signaling Tech.*) were added at final concentration of 0.5–2 μg/mL to the tubes. The cells were incubated for 30 min at 4°C in dark and then washed 3 times by centrifugation. For routine analysis cells were fixed with 2% paraformaldehyde for 10 min before FACS using FACSCelesta (*Beckton-Dickinson*) and the cell sorting was performed using $5 \cdot 10^6$ live cells labeled with anti-EGFR Fab'-AF647 antibody fragment (3–4 μg/mL) on a FACSAria IIu cell sorter (*Beckton-Dickinson*). Cells were sorted to obtain 4 subpopulations from the lowest to the highest fluorescence intensity corresponding to EGFR expression on the surface of transfected cells. Two populations with the lowest intensity (P1 and P2) of MDA-MB 231 dCas9 KRAB-T1.1 and MDA-MB 231 dCas9 KRAB-T2.1 were expanded via cell culture in the presence of hygromycin/puromycin and used for subsequent experiments.

Cell culture experiments

Fluorescence microscopy experiments were performed by growing WT and CRISPRi-attenuated MDA-MB 231 cells on glass coverslips to 75–80% confluency. Live cells were labeled directly with the Alexa Fluor 488, 647 or IRDye 800CW conjugated primary antibodies or their fragments for 30 min or 16 h (overnight) diluted 1:200-1:400 in 5%FCS FluoroBrite DMEM (*Thermo-Fisher*) supplemented with 25 mM HEPES, 4 mM glutamine and penicillin/streptomycin, pH 7.4. Cells were washed, fixed with 2% paraformaldehyde for 10 min and mounted in Vectashield (*Vector labs*) containing DAPI. Non-stained cells or cells incubated with the non-specific mouse IgG labeled with the corresponding fluorophore were used in control experiments. Bingeing and uptake of IRDye-labeled conjugates was investigated by plating cells in 12-well plates and incubating with anti-EGFR Fab'-800CW conjugate diluted in 5%FCS in FluoroBrite DMEM in the concentration range of 100–0.1 nM 800CW linked to Fab' or corresponding concentration of fluorescent labeled conjugate. In control wells to block endocytosis (probe internalization) the cells were pre-treated with 1 mM N-ethylmaleimide in complete medium for 2 min prior to adding the diluted probe. Plate-attached cells were incubated with IRDye 800CW-labeled conjugates for 0.25–1.5 h at 37°C with mixing in the dark. To test the specificity of cell binding a 5--fold excess of non-labeled Fab'2 cetuximab fragment was added to the incubation medium together with Fab'-800CW probe. Upon completion of incubation at various time points the cells were washed 2× with 5%FCS/FluoroBrite DMEM, 3x with DPBS and lysed by adding 0.2 mL of LysisB. Plates were sealed and cell lysates were treated by ultrasound in a sonication bath (2 min, RT, max power). Lysates were transferred to the wells of Greiner black 96-well plates with transparent wells containing 50 μL methanol/well and fluorescence intensity (800 nm emission) was read using Odyssey DLx Imager (*Li-Cor Corp*) and calibrated using IRDye 800CW standards diluted in the same buffer/methanol. Protein concentration was determined in each well by using Pierce detergent-compatible Bradford assay (*Thermo-Fisher*) and the uptake was normalized by cell lysate standards ($50\text{-}300 \cdot 10^5$ cells/50 μL).

Western blotting experiments were performed by transferring SDS-PAGE (4–15% gradient) resolved cell lysates (5-10 μg total cell lysate/lane) obtained by lysing cells in the presence of LysisB (1%Triton X-100, 0.1% SDS, 10% glycerol, 10 mM HEPES, 0.1 M NaCl, pH 7.0 containing cOmplete EDTA-free Protease inhibitor cocktail, *Millipore-Sigma*). EGFR was identified on the blots by using $F(ab')_2$-HRP conjugate[11] with subsequent detection of cell-bound peroxidase activity. Alternatively, anti-EGF Receptor (D38B1) XP Rabbit mAb (#4267, *Cell signaling Technology*), anti-GAPDH antibody (mAb 6C5, *Santa Cruz Biotechnology*) were used for detection essentially as described in Taghian et al.[57] Membranes were incubated with secondary goat anti-rabbit alkaline phosphatase conjugate (*Sigma*) diluted at 1:1500 in 0.1xTBS-B. Membranes were developed using NBT-BCIP solution (*Sigma-Aldrich*) diluted in 2 mM $MgCl_2$ in TBS, pH 9.5. Signals were analyzed as integrated intensities using Fiji/ImageJ software (NIH).

RNA probe design, synthesis, and Northern blotting

WT MDA-MB 231 cells were harvested at near 80% confluency and total RNA was extracted using Qiagen RNeasy Mini Kit (Cat. # 74104). First cDNA strand was synthesized using Maxima First Strand cDNA Kit with dsDNAse (Thermo Scientific Cat #K1671), DNA template was amplified by PCR using GoTaq Colorless Master Mix (Promega M 7132) using the following primer sequences: primer pair 1–5′ CCAGGAGGTG GCTGGTTATG 3′ (forward) and 5′ CTGTATTTGCCCTCGGGGTT 3′ (reverse), primer pair 2–5′ AAACACCGCAGCATGTCAAG 3′ (forward), 5′ ACAGTTGGGCCTGGATGAAC 3′ (reverse). The resultant DNA templates (0.612 kb or 1.531 kb, respectively) were purified using 1% agarose gel EF, DNA bands were excised and isolated by using High Pure PCR Product Purification Kit (*Roche*). For cloning of the purified DNA templates, pGEM-T Easy Vector System (*Promega*) was used by following the manufacturer's instructions. A 3:1 M ratio of the control insert DNA to the vector was used for the ligation and JM9 competent cells were transformed using the resultant plasmid and ampicillin/IPTG/X-Gal selection. Five blue colonies containing the insert (lacZ α-peptide sequence is disrupted by cloning into the pGEM-T Easy vector multiple cloning site) were picked, expanded, and purified plasmids were sequenced to check the orientation the inserts. The plasmids were linearized using suitable restriction enzymes (NEB Nco1-HF Cat. #R3193S or Sal1 Cat. #R3138S) and DIG-labeled riboprobe was synthesized using Promega Riboprobe synthesis kit (P1460) following the manufacturer's instructions. For synthesis of DIG labeled riboprobe, DIG-11 UTP Roche (Cat # 11209256910) was added at a ratio of 35:65 to unlabeled UTP in the Riboprobe synthesis mix. MDA-MB 231WT and EGFR CRISPRi cell lines T1.1 and T2.1 cells were grown in DMEM/10% FBS in the presence of hygromycin (500 μg/ml) and puromycin (0.5ug/ml). Total RNA was isolated using RNeasy Mini Kit (*Qiagen*) as described in manufacturer's instructions. Isolated RNAs were aliquoted and stored at −80C. For Northern blot analysis 2.0 μg of total RNA isolated from each cell line was electrophoresed on a 1% agarose gel containing 2 M formaldehyde. RNA from the gel were transferred to a nylon membrane (Hybond XL, Amersham). RNA was UV-cross-linked to the membrane and transferred to hybridization bottle and 3–5 mL of pre warmed hybridization solution (Thermo-Fisher Scientific, ULTRAhyb Ultrasensitive Hybridization Buffer, Cat. No. AM8670). After a 30 min pre-hybridization buffer was replaced with the hybridization buffer containing digoxigenin-labeled RNA probe (50 ng/mL) and hybridized overnight at 68°C. The blots were washed 2 × 5 min in 2X SSC, 0.1% SDS and then 2 × 15 min in 0.1X SSC, 0.1% SDS at 68°C under constant agitation. After hybridization and stringency washes the membrane was rinsed briefly with maleic acid washing buffer containing 0.3% (v/v) Tween 20. Membrane was blocked for 30 min in 1.0% blocking solution in maleic acid buffer followed by incubation in 150 mU/mL of anti-DIG AP-antibody conjugate in blocking buffer for 30 min. The membrane was washed 2 × 15 min in washing buffer followed by 2–5 min equilibration in 0.1M Tris/NaCl pH 9.5 detection buffer. The membrane was placed in a development folder, covered with 0.25M CPD Star substrate (Invitrogen Cat #T2146) and incubated for 5 min at room temperature. Excess liquid was removed, and the edges were heat sealed. The damp membrane was incubated at 37°C for 10 min. The membrane was imaged using Bio-Rad ChemiDoc MP Imaging System.

Fluorescence microscopy

Imaging of cells and tumor sections was performed by using DM8 Fluorescent microscope fitted with SOLAnIR Light Engine (Leica), or TE2000-U inverted microscope (Nikon) equipped with a dual 100W Dia-illuminator/M780L3-C5(780 nm), 170 mW collimated LED (ThorLabs) light sources. In some experiments the samples were subjected to FLIM as described below.

Fluorescence lifetime microscopy (FLIM)

Stellaris 8 Falcon FLIM confocal system (Leica) for NIR FLIM in time-domain time-correlated single photon counting mode was used essentially as described in Pal et al.[20] at 730-nm excitation with 750-nm notch filter with HyD R detection (770-850-nm) with 4-line repetitions/averages. A 10×, 0.4 NA objective was used for image collection and digital images with 512 × 512 pixels (2.275 μm/pixel) per frame. All samples (cell culture and frozen sections) were fixed for 10 min in 4% formaldehyde in 25 mM HEPES/HBSS, pH 7.4, washed in HBSS and mounted in SlowFade Glass (Thermo-Fisher).

Widefield Fluorescence lifetime TD imaging

A custom-built time domain (TD) fluorescence imaging system was used for *in vitro* imaging. The TD imaging system consisted of a portable cart with a pulsed laser source (EXR-20, SuperK Varia, NKT Photonics, repetition rate: 80 MHz; tuning range: 400–850 nm) providing 770 ± 30-nm excitation. The excitation light was delivered to the sample using a multimode fiber (Thorlabs, Newton, New Jersey, United States) connected to a digital micromirror device (DMD), and fluorescence emission was collected in the reflectance mode using an 835 ± 70-nm band-pass filter (AVR Optics). TD fluorescence images were captured using a gated intensifier (Picostar, LaVision) and a CCD camera (LaVision, Picostar, 500 V gain, 0.1 to 1 s integration time, 256 × 344 pixels after 4 × 4 hardware binning). Imaging was performed with a 500 V gain, 500 ps gate width, and 150 ps steps for a total duration of approximately 6 ns per laser duty cycle of 12.5 ns.

Mouse model

Tumor growth and mouse imaging was performed according to UMASS Chan IACUC approved animal protocol. Wild-type MDA-MB-231 and T2.1 cells were grown culture to sub-confluent density, treated with TryPLE Express reagent and implanted in serum-free medium containing 10% Matrigel (Beckton-Dickinson) into mammary abdominal fat pad.[58] It took 48 ± 12 days for both control (WT) and attenuated (T2.1) mammary TNBC tumors to reach the volume of 0.6–1.0 cm^3. Randomized animals (female J:NU mice, The Jackson Laboratory Stock 007850, 5–6 weeks, n = 6/group) were injected with 800CW labeled cetuximab Fab' at the dose of 60–65 μg/mouse (1.2 nmol/mouse, 3.6 nmol

800CW, approximately 180 nmol 800CW/kg) in 0.15 mL of sterile DPBS. Intravenous injections were followed by FI imaging (IVIS Spectrum/CT (PerkinElmer), at 0.5, 3 and 24 h) using a xenon lamp or 750 nm laser diode excitation sources. The animals were subjected to imaging using in 2D mode with $1.2.10^4$-$2.0{\cdot}10^4$ photon counts collected over 0.5–1 s. Manually drawn ROI analysis was used in quantifying average photon counts for comparing various time points. Animals were additionally imaged in 3D image acquisition mode to obtain CT-corrected maximum intensity projection (MIP) images. These images were analyzed using volume-rendered ROIs.

RNA extraction and qRT-PCR analysis

Extraction of total RNA from the tissue samples (n = 4/group) was performed in 0.15 mL of 1× proteinase K digestion buffer (20 mM Tris-HCl, pH 8.0; 1 mM $CaCl_2$, 0.5% sodium dodecyl sulfate) containing 500 μg/mL proteinase K. Samples were suspended in the buffer by vortexing and incubated at 55°C for 3 h in a water bath. One mL TRIzol (*Thermo-Fisher*) was added, incubated for 5–10 min and extraction with 0.2 mL chloroform was performed. Total RNA was precipitated from water phase at −20°C in the presence of glycogen, washed with 100% ethanol, air-dried at room temperature, and then dissolved in RNAse-free water. The extracted RNA was used immediately to synthesize cDNA or stored at −80°C for later use. First strand cDNA was synthesized using the HiFi 1st Strand cDNA synthesis kit (*101 Bio.com*) following the manufacturers protocol. The newly synthesized cDNA was stored at −20C. Exon junction spanning primers (EGFR forward primer 5′-CCCCCT GACTCCGTCCAGTA-3′, reverse primer: 5′-CTCGTGCCTTGGCAAACTTTC-3′; GAPDH forward primer: 5′- GACAGTCAGCCGCATCT TCT-3′, reverse primer 5′-TTAAAAGCAGCCCTGGTGAC-3′) were generated using Primer-Blast (NCBI-NIH) with specificity checking against rodent genomes database. qPCR was performed using Bio-Rad 1000 series Thermal cycler (*Bio-Rad*). 20-μL reactions were conducted in triplicates, containing 0.4 μM of each primer in a 96 well plate using Ultra SYBR Green qPCR master mix (2×, with ROX 1, 101 Bio.com). Cycling conditions were as follows: 95°C for 10 min initial denaturation, followed by 40 cycles of denaturation (95°C for 15 s), annealing (55°C for 30 s) and extension (70°C for 30 s).

Histology and immunohistochemistry

Tumors were excised post euthanasia, rinsed in ice-cold saline and embedded in OCT by snap-freezing immediately post resection. Thin frozen sections (8 μm thick) were fixed in acetone (−20°C). After washing in TBS (50 mM Tris, 100 mM NaCl, pH 7.4) sections were blocked using 5% calf serum in TBS for 1 h. A mixture of primary antibodies (InVivoMAb anti-human PD-L1 (B7-H1, *BioXCell*) custom labeled with digoxigenin NHS essentially as described in Shazeeb et al.,[6] and anti-CD31/PECAM-1 (MEC 13.3, *Santa Cruz*) diluted at 1:100 in 5% calf serum in TBS) was applied onto the sections and incubated for 2 h at RT. Control sections were incubated in the presence of an excess of non-labeled Cetuximab (0.2 mg/mL final concentration) with other primary antibodies omitted. Sections were washed 5× in 5% calf serum in TBS and incubated in the presence of a mixture of Cetuximab-AF647 (1.5 μg/mL), anti-rat IgG2a-AF488 (*SouthernBiotech*, diluted 1:50) and Cy3-labeled anti-digoxigenin Fab (*Millipore-Sigma*, concentration – 0.5 μg/mL) in 5% calf serum in TBS for 1 h. Sections were washed 5× in 5% calf serum in TBS, fixed in 4% formaldehyde in DPBS, pH 7.5 for 10 min and mounted using Vectashield with DAPI (*Vector Labs*).

QUANTIFICATION AND STATISTICAL ANALYSIS

The differences between the means of the blotting signals, SNR values reflecting imaging probe uptake values by individual cells vs. background were compared by using by Student's t test with Welch's correction (data normal distribution, no equal variances assumed). Tumor: background imaging signal ratios were compared between the groups of animals using non-parametric Mann-Whitney-Wilcoxon test. P of 0.05 was assumed significant for all tests.